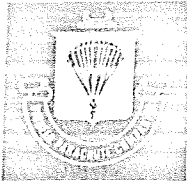


A Reproduced Copy  
OF

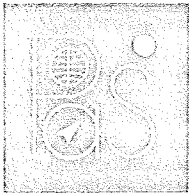
---

Reproduced for NASA  
by the  
**NASA** Scientific and Technical Information Facility

FACILITY FORM 602	N70-74728	
	(ACCESSION NUMBER)	(THRU)
	111	None
	(PAGES)	(CODE)
	CR-108464	
	(NASA CR OR TMX OR AD NUMBER)	(CATEGORY)



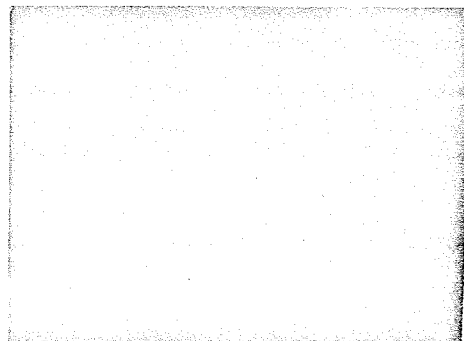
PIONEER PARACHUTE COMPANY



*a wholly owned  
subsidiary of*

**Pioneer Aerodynamic Systems, Inc.**

*Manchester, Conn.*



IF ☐ OTHER  
OF DUP-CHECK CLERK

NASA CR 108467

H. G. Heinrich.  
Eugene L. Haak  
and  
Ronald J. Niccum

Department of Aeronautics and  
Engineering Mechanics  
University of Minnesota

April 1964

FINAL TECHNICAL REPORT  
PARA-SAIL EVALUATION AND DEVELOPMENT  
VOLUME I  
AERODYNAMIC INVESTIGATIONS  
OF PARA-SAIL PARACHUTES

Sponsored by the Pioneer Parachute Company, Inc. (Projects  
E-2038 and E-2067) under National Aeronautics and Space  
Administration Contract NAS 9-1157

DISTRIBUTION

NASA, Manned Spacecraft Center  
Procurement and Contracts Division  
General Research Procurement Office  
Houston 1, Texas  
Attn: Jack H. Goldstein

(1) Copy

Maj. James E. Ballweg (FTOP)  
Hdqs. AFFTC, Plans & Programs Division  
Edwards Air Force Base, California

(1) Copy

Mr. James V. Waite, (FTLGR)  
6511th Test Group (P)  
El Centro Naval Air Station  
El Centro, California

(1) Copy

NASA Manned Spacecraft Center  
Houston, Texas  
Attn: Marvin F. Matthews  
Patent Counsel

(1) Copy

NASA, Manned Spacecraft Center  
Mechanical System Branch  
Building 13  
Clear Lake City  
Houston, Texas  
Attn: Leland Norman

(6) Copies

University of Minnesota  
Department of Aeronautics  
and Engineering Mechanics  
Minneapolis 55, Minnesota  
Attn: Dr. Helmut G. Heinrich

(5) Copies

Pioneer Parachute Company, Inc.

Sales Department

(1) Copy

Engineering Department

(4) Copies

## FORWARD

In January of 1963, Pioneer Parachute Company, Inc., under National Aeronautics and Space Administration Contract NAS 9-1157, undertook a program of evaluation and development of a large Para-Sail Parachute capable of recovering heavy payloads and providing a significant degree of gliding and maneuvering characteristics. In March 1964 all test work under this contract was successfully completed.

In the course of this program the principle aerodynamic coefficients for this type of parachute were established in wind tunnel tests. Utilizing the wind tunnel as an investigative tool, studies were made of methods to improve upon these coefficients and to establish better inflation characteristics. These efforts were performed by the University of Minnesota, Department of Aeronautics and Mechanics, and are reported in Volume I of this document, entitled "Aerodynamic Investigations of Para-Sail Parachutes".

The results of the wind tunnel experiments were validated by a series of full scale developmental drop tests with a Para-Sail of approximately 80 feet in diameter. These tests were conducted at the Joint Parachute Test Facility, El Centro, California, and are described in Volume II of this report, "Design and Testing of a Large Para-Sail Parachute".

PIONEER PARACHUTE COMPANY, INC.

## ABSTRACT

Wind tunnel studies were performed on a gliding parachute, called Para-Sail, with the objective of deriving a configuration that would provide a lift to drag ratio of unity or greater combined with a strong opening tendency and sufficient static stability about the pitch, roll and yaw axes. According to model experiments, this objective has been achieved.

Upon request of the Pioneer Parachute Company, Manchester, Connecticut, and the NASA Center for Manned Space Flight, Houston, Texas, several additional aerodynamic aspects such as the center of pressure, suspension line forces, the effect of air-catching scoops and the internal parachute upon the opening characteristics have also been investigated.

The study was sponsored by the Pioneer Parachute Company, with Messrs. Edward A. Gimalouski and William J. Everett acting as project engineers. The experiments and the analysis were carried out, and a number of modifications were proposed by the staff of the Department of Aeronautics and Engineering Mechanics, University of Minnesota. Messrs. Thomas C. Nietz, Harvey M. Lipka and Lelan R. Jamison, students of Aerospace Engineering, contributed significantly to the completion of this study.

# TABLE OF CONTENTS

	PAGE
I. Introduction . . . . .	1
II. Models . . . . .	4
III. Notation . . . . .	20
IV. Configuration I . . . . .	26
A. Investigation of Original Para-Sail . . .	26
B. Modification of the Para-Sail Configuration . . . . .	53
V. Investigation of Configuration II . . . . .	65
VI. Investigation of Configurations III and IV .	75
A. Configuration III . . . . .	75
B. Configuration IV . . . . .	78
VII. Conclusions . . . . .	87
List of References . . . . .	93
Appendix . . . . .	94

# LIST OF FIGURES

	PAGE
1. Schematic Representation of the Forces Acting Upon a Parachute in Free Descent . . . .	2
2. Para-Sail Configuration I Model Drop Test . . . . .	5
3. Para-Sail Configuration I Wind Tunnel Test . .	7
4. Schematic Planform of Configuration I and Suspension Line Lengths . . . . .	8
5. Schematic Planform and Suspension Line Lengths of Para-Sail Configuration II . . . . .	9
6. Schematic Profile of Para-Sail, Configuration II . . . . .	10
7. Para-Sail Configuration II Wind Tunnel Test . .	11
8. Para-Sail Configuration II Model Drop Test . .	12
9A. Schematic Planform and Suspension Line Lengths of Para-Sail Configuration III . . . .	13
9B. Dimensionless Gore Patterns for Solid Front Panels of Configuration III . . . . .	14
10. Para-Sail Configuration III Wind Tunnel Test .	16
11A. Schematic Planform and Suspension Line Lengths of Para-Sail Configuration IV . . . .	17
11B. Dimensionless Gore Patterns for Solid Front Panels of Configuration IV . . . . .	18
12. Para-Sail Nomenclature . . . . .	21
13. Para-Sail Nomenclature . . . . .	22
14. Location of Lines for Para-Sail . . . . .	23
15. Stability Notation for Gliding Parachute . .	24
16. Flow Field About Para-Sail . . . . .	27
17. Subsonic Wind Tunnel Test Arrangement for Pendulum Tests . . . . .	29

# LIST OF FIGURES (Cont.)

	PAGE
18. Close-up of Pendulum and Angle Measuring Device . . . . .	30
19. Pendulum Testing Arrangement and Recording Equipment . . . . .	31
20. Typical Oscillograph Recording of Motion of a Parachute in Pendulum Tests . . . . .	32
21. Stable Angle of Attack Vs Velocity for Configuration I with Various Nominal Porosities . . . . .	34
22. Prototype Para-Sail (I-24-4.67 During Three Component Tests . . . . .	36
23. Moment Coefficient Vs Angle of Attack for Configuration I (Based on Total Surface Area $S_0$ , Reynolds Number = $8 \times 10^5$ , $D_0 = 24"$ ) . . .	37
24. Normal Force Coefficient Vs Angle of Attack for Configuration I (Based on Total Surface Area $S_0$ , Reynolds Number = $8 \times 10^5$ , $D_0 = 24"$ ) . . . . .	38
25. Tangent Force Coefficient Vs Angle of Attack for Configuration I (Based on Total Surface Area $S_0$ , Reynolds Number = $8 \times 10^5$ , $D_0 = 24"$ ) . . . . .	39
26. Moment Coefficient Vs Angle of Attack for Model I-24-4.67 with Variations in the Front Riser Lengths (Based on Total Surface Area $S_0$ ). . . . .	40
27. Normal Force Coefficient Vs Angle of Attack for Model I-24-4.67 with Variations in the Front Riser Length (Coefficients Based on Total Surface Area $S_0$ ) . . . . .	41
28. Tangent Force Coefficient Vs Angle of Attack for Model I-24-4.67 with Variations in the Front Riser Length (Coefficients Based on Total Surface, $S_0$ ) . . . . .	42
29. Moment Coefficient Vs Angle of Attack for Model I-24-4.67 with Variation in the Centerline Length (Coefficients Based on Total Cloth Area $S_0$ ) . . . . .	43

# LIST OF FIGURES (Cont.)

	PAGE
30. Normal Force Coefficient Vs Angle of Attack for Model I-24-4.67 with Variation in the Centerline Length (Coefficients Based on Total Cloth Area $S_0$ ) . . . . .	44
31. Model Suspension for Measuring Normal Force and Tangent Force . . . . .	46
32. Model Suspension and Strain Gage Balance Arrangement for Measuring Normal Force and Tangent Force . . . . .	46
33. Forces and Coordinates Used for Determining Aerodynamic Coefficients . . . . .	47
34. Subsonic Wind Tunnel Test Arrangement for Line Tension Tests . . . . .	51
35. Schematic Planform of Configuration I Showing Suspension Line Adjustments for a 5 x 7 Line Configuration . . . . .	54
36. Line of Action of Riser Forces and Resultant Force (A.C.L.) of a Para-Sail Prototype (Derived from a 32" $D_d$ Model in Pendulum Test) . . . . .	55
37. Para-Sail (I-48-47) with Modified Apex $\alpha = 34^\circ$ , $L/D = .67$ . . . . .	57
38. Front View of Para-Sail (I-48-47) with Portions of Gores . . . . .	58
39. Rear View of Para-Sail (I-48-47) with Portions of Gores . . . . .	60
40. Para-Sail (I-48-47) With Stabilization Panels Removed ( $\alpha = 40^\circ$ , $L/D = .84$ ) . . . . .	61
41. Final Form of Modified Para-Sail (I-32-4.67) ( $\alpha = 47^\circ$ , $L/D = 1.07$ ) . . . . .	63
42. Dimensionless Gore Pattern for Front of Configuration II . . . . .	66
43. Dimensionless Gore Pattern for Rear Skirt Panels of Configuration II . . . . .	67

# LIST OF FIGURES (Cont.)

	PAGE
44. Stable Angle of Attack Vs Velocity for Configuration II for Various Nominal Porosities . . . . .	68
45. Para-Sail Configuration II (II-24-4.67) During Three Component Studies . . . . .	69
46. Para-Sail Configuration II (II-24-4.67) During Three Component Studies (Note Elliptical Profile) . . . . .	70
47. Normal Force Coefficient Vs Angle of Attack for Configuration II (Based on Total Surface Area $S_o$ , Reynolds Number = $8 \times 10^5$ , $D_o = 24''$ ) . . . . .	71
48. Moment Coefficient Vs Angle of Attack for Configuration II (Based on Total Surface Area $S_o$ , Reynolds Number = $8 \times 10^5$ , $D_o = 24''$ ) . . . . .	72
49. Tangent Force Coefficient Vs Angle of Attack for Configuration II (Based on Total Surface Area $S_o$ , Reynolds Number = $8 \times 10^5$ , $D_o = 24''$ ) . . . . .	73
50. Test Section and Model Support for Opening Shock Program (Infinite Mass Case) . . . . .	76
51. Para-Sail Configuration III (III-48-4.67) in Reefed Condition for Opening Shock Tests in the Wind Tunnel . . . . .	79
52. Aerodynamic Centerline (A.C.L.) and Parachute Centerline (P.C.L.) of Model III-48-4.67 with an Unattached Centerline (5 x 7 Line Configuration $V_\infty = 30$ ft/sec) . . . . .	80
53. Inflation of the Reefed Para-Sail with, and without, Center Lines . . . . .	84
54. Aerodynamic Center Line (A.C.L.) and Parachute Center Line (P.C.L.) of Model IV-48-4.67 with and Unattached Center Line (9 x 9 Line Configuration $V_\infty = 30$ ft/sec) . . . . .	86

# LIST OF FIGURES (Cont.)

	PAGE
55. Stable Angle of Attack Vs Velocity for Configurations I and II for Various Nominal Porosities . . . . .	88
56. Results of Modifications of Prototype Para-Sail I-48-47 . . . . .	89
57. Results of Modifications of Prototype Para-Sail I-48-47 . . . . .	90
58. Results of Modifications of Prototype Para-Sail I-32-4.67 . . . . .	91
59. Results of Modifications of Prototype Para-Sail I-32-4.67 . . . . .	92
60. Planform of the Inflated 80 Ft Para-Sail . . .	95
61. Profiles of the Inflated 80 Ft. Para-Sail . . .	96
62. Photographs of a Reefed Para-Sail Configuration IV With Center Line (1.035 D <sub>0</sub> ) .	98
63. Photographs of a Reefed Para-Sail Configuration IV Without Center Line . . . . .	99

## LIST OF TABLES

PAGE

I.	Ratio of Line Force to Total Force for Model I-32-4.67 with Different Front Riser Lengths . . . . .	52
II.	Stable Angle of Attack of Model IV-48-4.67 with Variations in the Center Line Length and Number of Front Scoops ( $V_{\infty} = 25$ fps) . . . . .	82

# LIST OF SYMBOLS

$C_M$	moment coefficient
$C_N$	normal force coefficient
$C_T$	tangent force coefficient
$D$	drag = $C_D \frac{1}{2} V^2 S_o$
$D_d$	design diameter of main canopy
$D_o$	nominal diameter of Para-Sail (based on total canopy area, $S_o$ , estimated from a model furnished by Pioneer Parachute Company)
$K$	canopy moment arm
$L$	lift
$q$	dynamic pressure = $\frac{1}{2} \rho V^2$
$S_o$	total canopy area (estimated) including stabilization panels
$\alpha$	angle of attack = $\tan^{-1} L/D$ (measured against vertical)
(5x7)	five suspension lines attached to each front riser and seven suspension lines to each back riser
(6x6)	six suspension lines attached to each front riser and six suspension lines attached to each back riser

## I. INTRODUCTION

With many conventional parachutes, the stable angle of attack is such that the parachute develops lift as well as drag. When this occurs, the parachute is said to glide or to fly at an angle of attack. The angle of attack,  $\alpha$ , is determined by the ratio of the lift and drag forces,  $L/D$ , and it can be seen from Fig 1 that

$$\alpha = \text{TAN}^{-1} (L/D) \quad (1)$$

When steadily gliding, the aerodynamic forces of the parachute and the suspended weight are in equilibrium. In order to maintain the position of equilibrium, the forces acting on the canopy when deflected, must develop a so-called restoring moment which tends to move the canopy towards its stable position.

The objectives of this study were to establish the aerodynamic characteristics of the gliding parachute called the Para-Sail and to try through modification to obtain a relatively high lift to drag ratio, if possible, exceeding unity. In view of these and additional objectives, this study was pursued in the following three principal aspects.

1. Investigation of the original Para-Sail configuration including the following major items:
  - a) Exploration of flow field about the canopy
  - b) Effect of the suggested slots, louvers, center lines, stabilization panels and porosity upon the lift to drag ratio

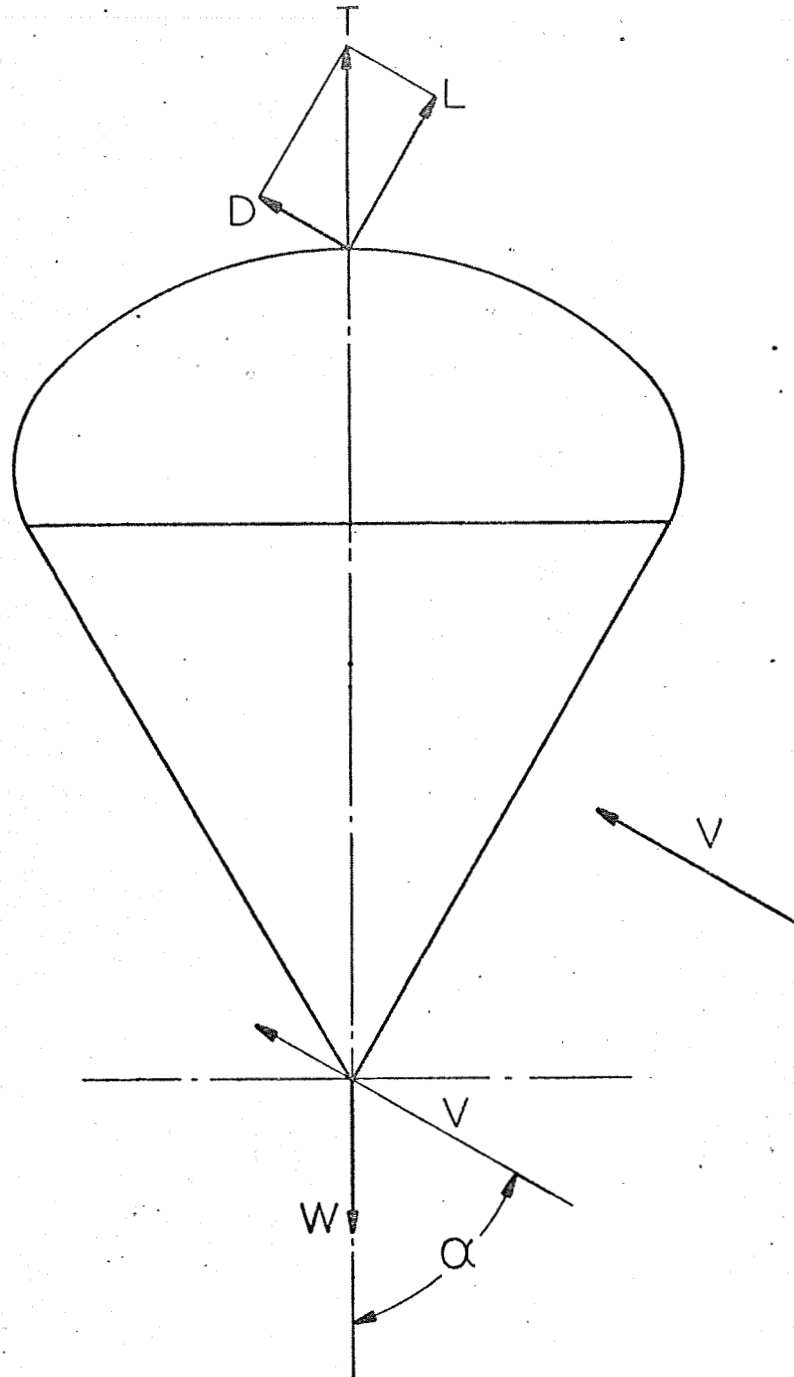


FIG 1. SCHEMATIC REPRESENTATION OF THE FORCES ACTING UPON A PARACHUTE IN FREE DESCENT

- c) Three-component measurements to determine the aerodynamic coefficients
  - d) Measurement of riser and center line forces and determination of the center of pressure.
- 2. Modification of the Para-Sail configuration to increase the lift to drag ratio.
- 3. Investigation of the modified Para-Sail configurations, in particular, the following major items:
  - a) Methods to vary the lift to drag ratio through suspension line adjustment
  - b) Three-Component measurements to determine the aerodynamic coefficients.

In addition to these objectives, it became necessary to perform a number of model tests related to operational performance characteristics, which were either observed during full size drop tests or which were thought to be advantageous for actual applications. Therefore, it became necessary to perform certain experiments seemingly incomplete or out of sequence. The results of these particularly requested experiments are arranged in the appendix.

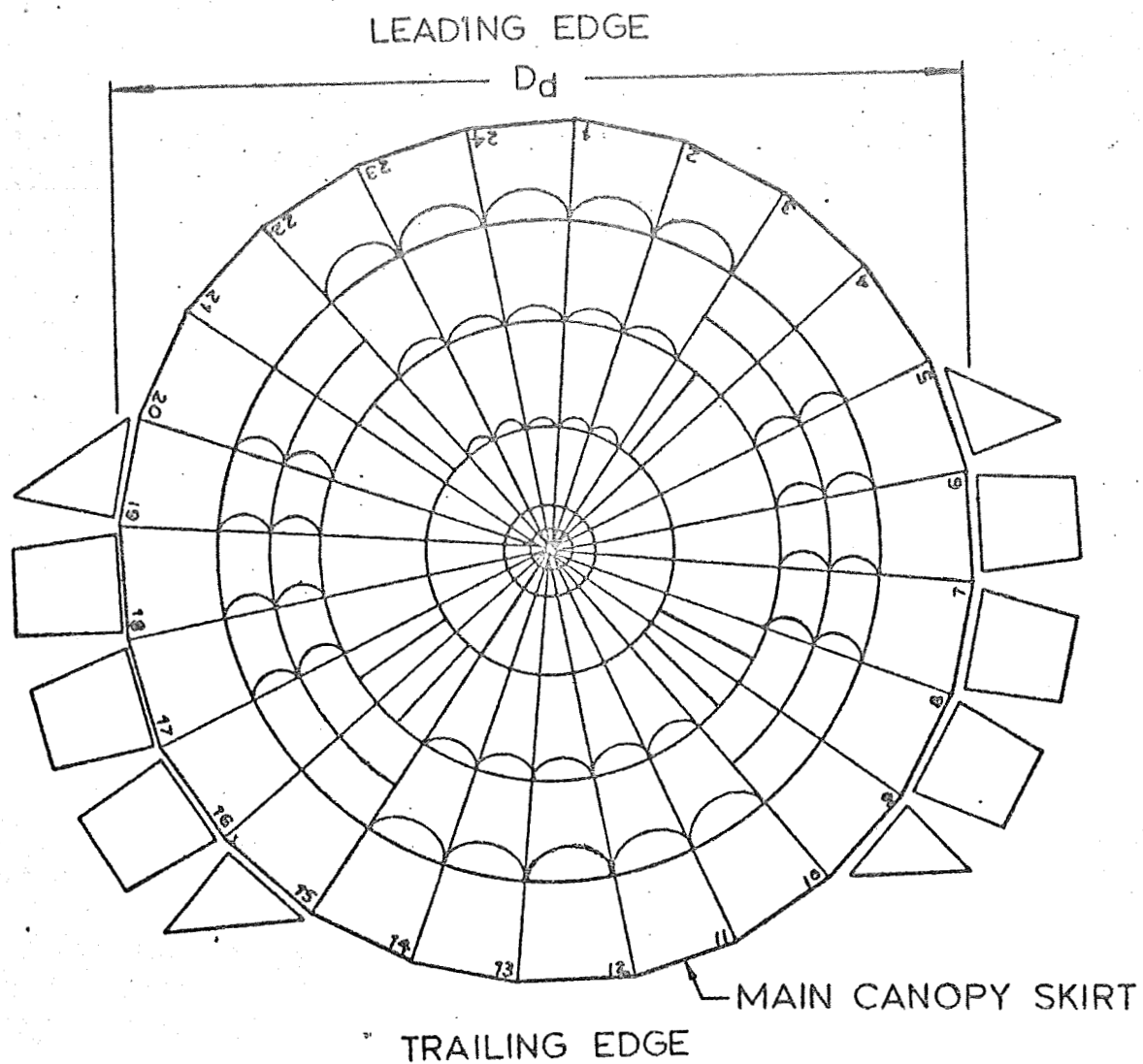
## II. MODELS

Four principal configurations of the Para-Sail have been investigated in this study.

Configuration I is the prototype Para-Sail as proposed by Mr. Lemoigne and redesigned by the Pioneer Parachute Company, Manchester, Connecticut. For simplicity in the model tests, the suspension lines were grouped in four equal bundles and then connected to four separate risers. Figures 2 and 3 show Configuration I in free flight and in wind tunnel tests. Figure 4 illustrates the planform and details of the suspension lines.

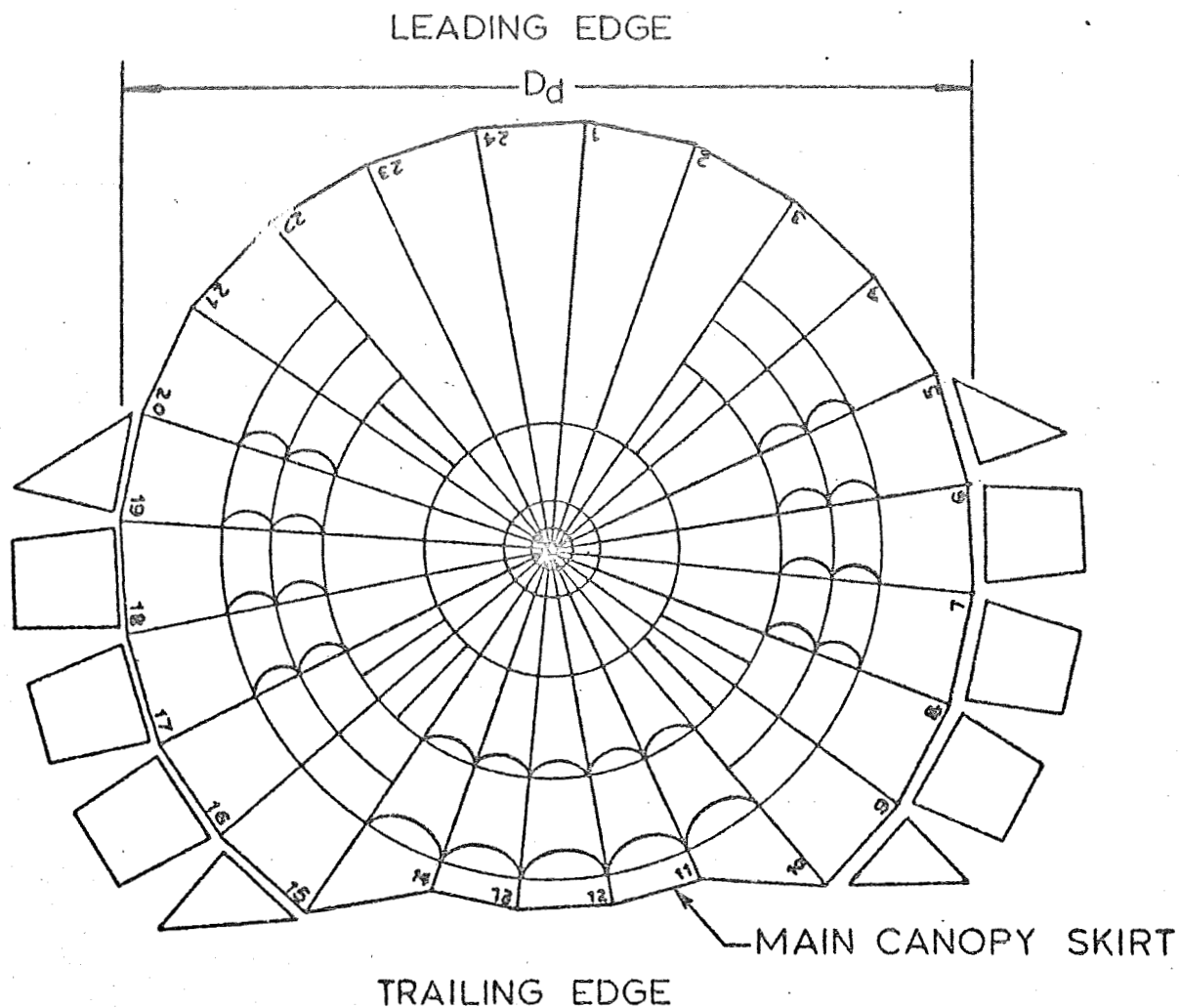
Configuration II was derived through modifications of Configuration I. The gores 1, 2, 22, 23 and 24 have been replaced by five solid gores similar to those of a solid flat circular canopy. Also, material has been removed in the skirt area from gores 10 through 14, which are located at the rear of the canopy. The suspension line lengths have been slightly changed as indicated in Fig 5. These changes resulted in a higher L/D ratio. Figures 5 and 6 are schematic drawings of the Para-Sail Configuration II, while Figs 7 and 8 show this configuration in the wind tunnel and during drop tests.

Configuration III has a solid front similar to Configuration II except that some of the material also has been removed from the leading edge of the canopy. A schematic view of Configuration III is shown in Figs 9A and 9B. These modifications resulted from the review of full size drop tests conducted jointly by the Pioneer Parachute Company and the NASA Center



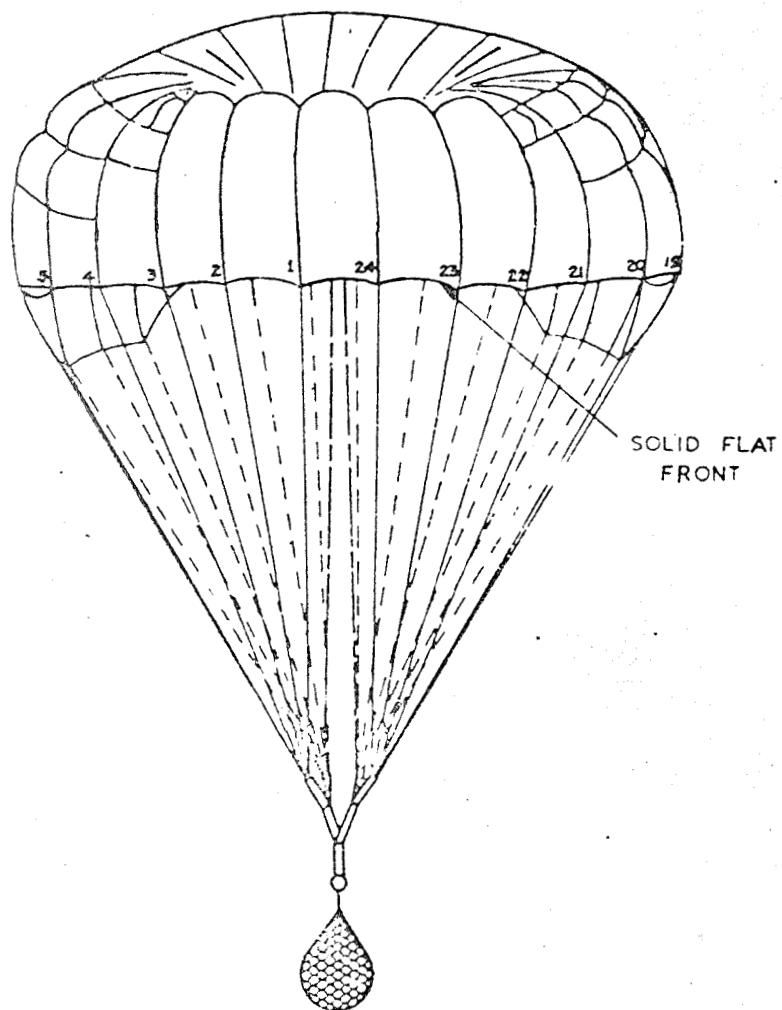
RISER	LINE NO.	LINE LENGTH (INCLUDING RISER)
RIGHT FRONT	( 1 → 6 )	1.00 $D_d$
LEFT FRONT	( 19 → 24 )	1.00 $D_d$
RIGHT REAR	( 7 → 12 )	1.00 $D_d$
LEFT REAR	( 13 → 18 )	1.00 $D_d$
—	CENTERLINE	0.92 $D_d$

FIG 4. SCHEMATIC PLANFORM OF CONFIGURATION I  
AND SUSPENSION LINE LENGTHS

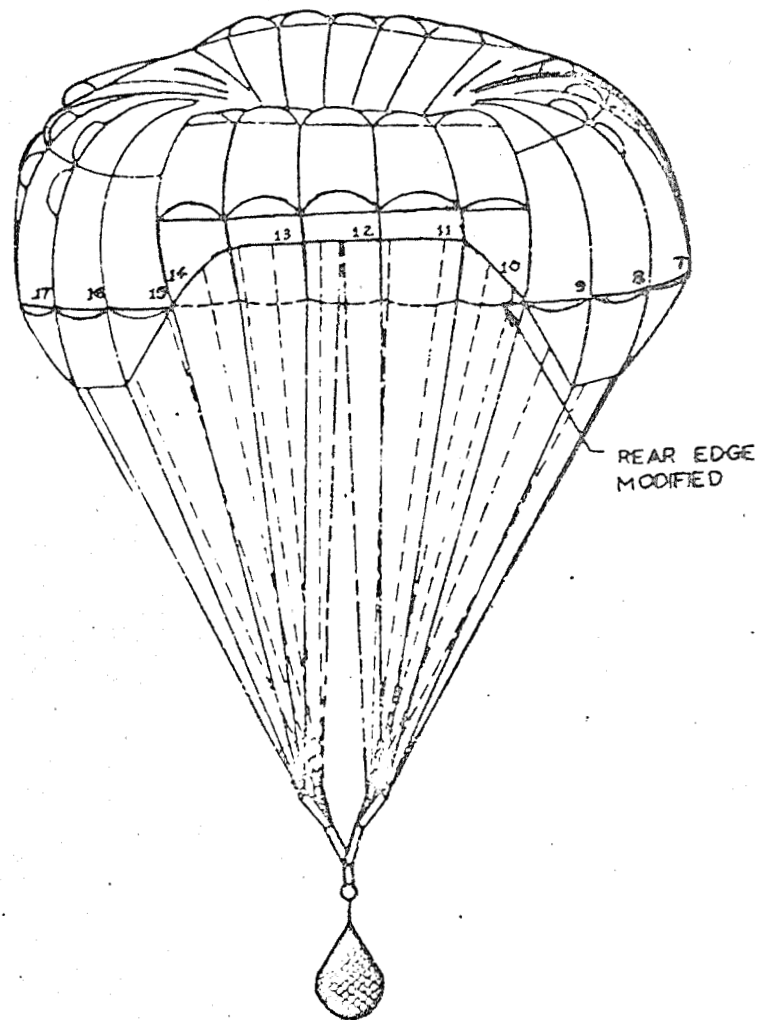


RISER	LINE NO	LINE LENGTH (INCLUDING RISER)
RIGHT FRONT	( 1 → 6 )	0.97 $D_d$
LEFT FRONT	( 19 → 24 )	0.97 $D_d$
RIGHT REAR	{ ( 7 → 10 )	1.00 $D_d$
	{ ( 11 → 12 )	1.02 $D_d$
LEFT REAR	{ ( 13 → 14 )	1.02 $D_d$
	{ ( 15 → 18 )	1.00 $D_d$
—	CENTERLINE	0.90 $D_d$

FIG 5. SCHEMATIC PLANFORM AND SUSPENSION LINE LENGTHS OF PARASAIL CONFIGURATION II

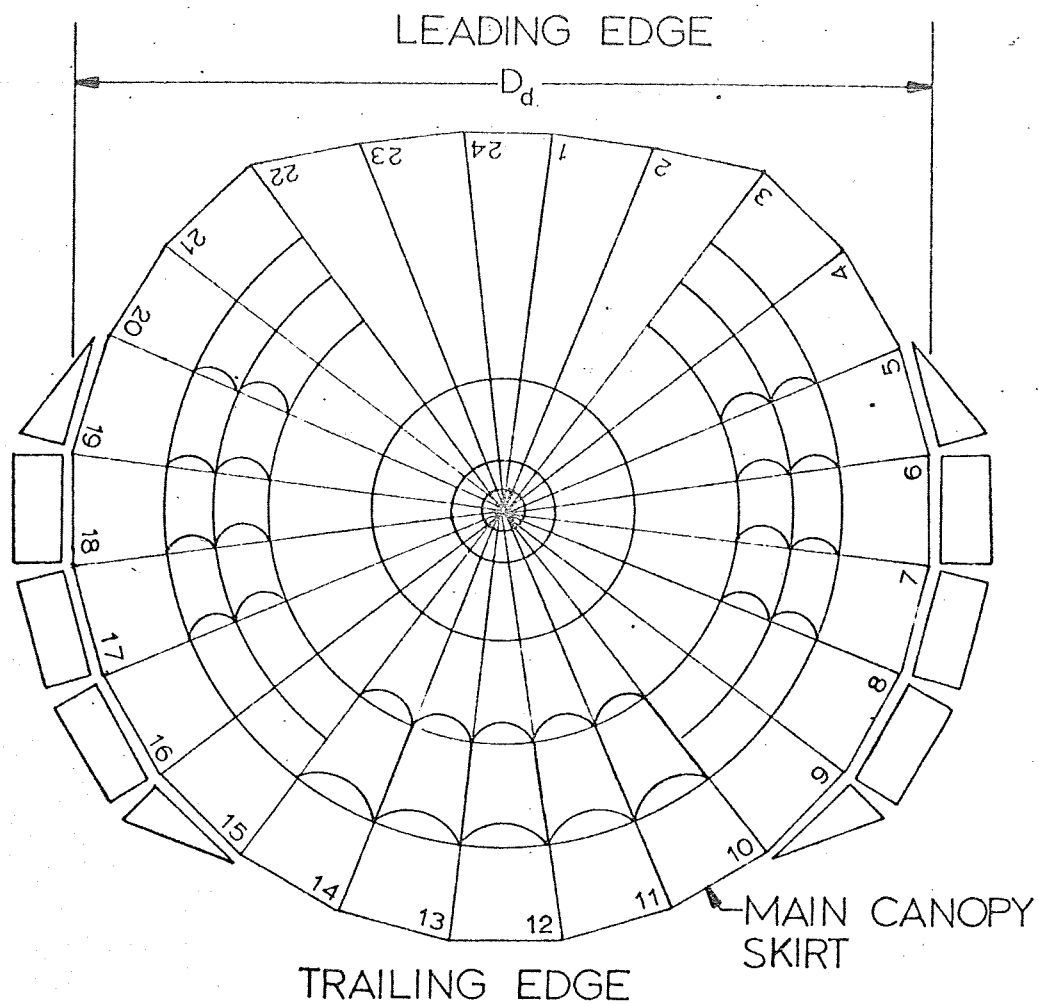


FRONT VIEW



REAR VIEW

FIG 6. SCHEMATIC PROFILE OF PARASAIL, CONFIGURATION II



RISER	LINE NO.	LINE LENGTH (INCLUDING RISER)
RIGHT FRONT	(1 → 6)	1.00 $D_d$
LEFT FRONT	(19 → 24)	1.00 $D_d$
RIGHT REAR	{ (7 → 10)	1.00 $D_d$
	{ (11 → 12)	1.00 $D_d$
LEFT REAR	{ (13 → 14)	1.00 $D_d$
	{ (15 → 18)	1.00 $D_d$
—	CENTERLINE	$D_d$

FIG 9A. SCHEMATIC PLANFORM AND SUSPENSION LINE LENGTHS OF PARASAIL CONFIGURATION III

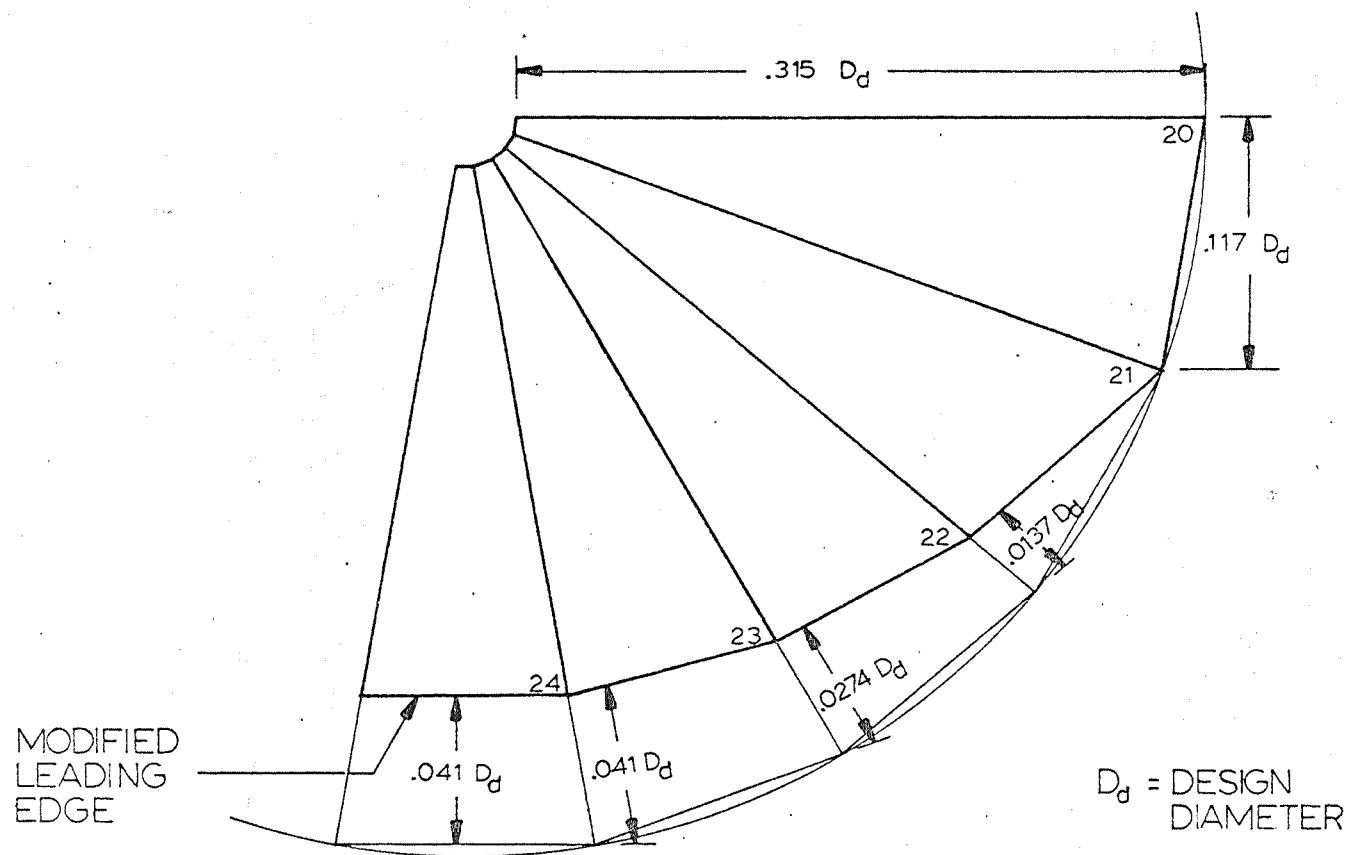


FIG 9B. DIMENSIONLESS GORE PATTERNS FOR SOLID FRONT PANELS OF CONFIGURATION III

for Manned Space Flight. Figure 10 shows a model of Para-Sail Configuration III in the wind tunnel.

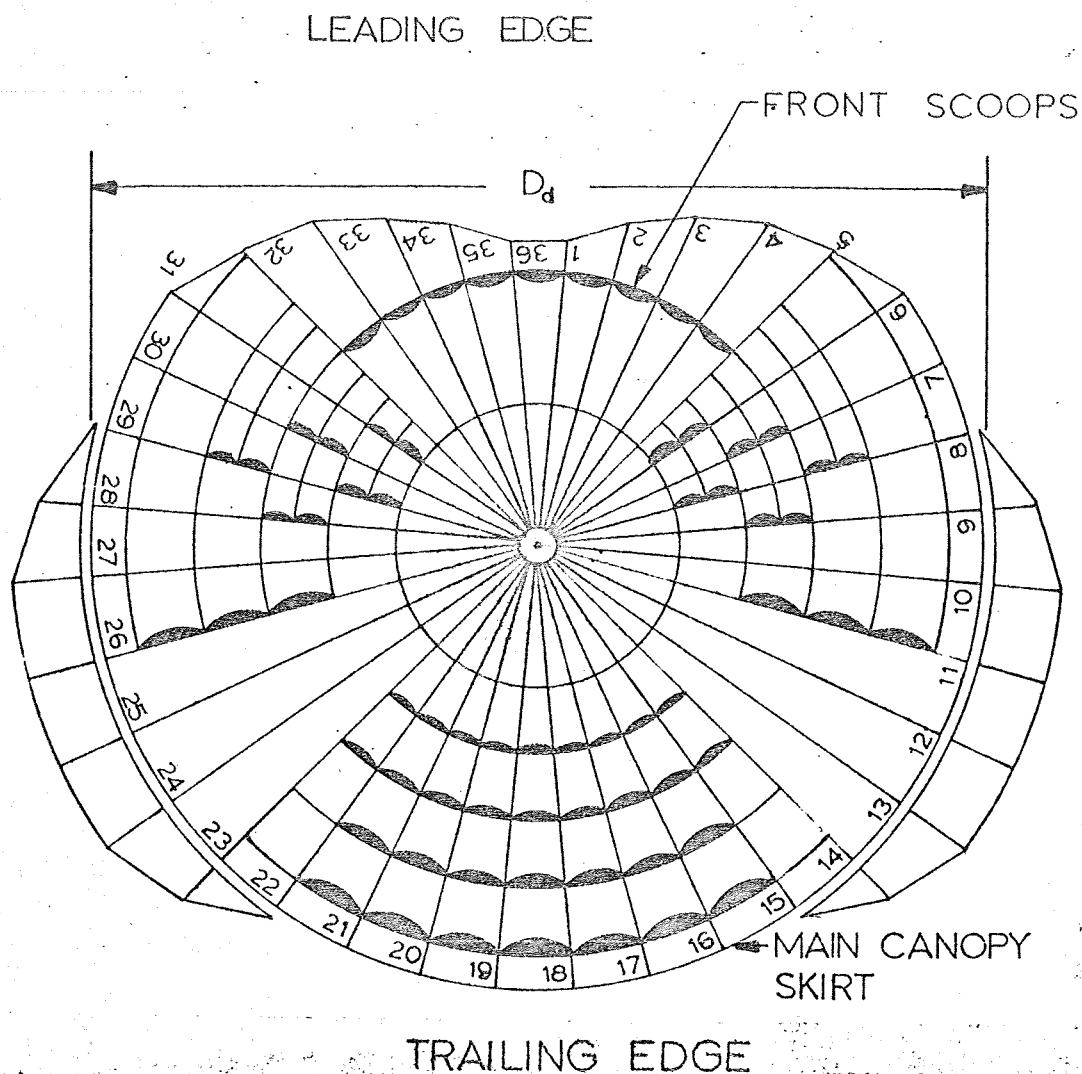
A version of this configuration has been tested by NASA Manned Space Flight Center, Houston, Texas, and details of these efforts are shown in Ref. 4.

Configuration IV is a model obtained from a scaling down process of a full size parachute called Para-Sail 80A. However, the model and the full size parachute have merely the plan form, to a certain extent, in common. This is particularly true for the removal of cloth at the leading edge and the so-called scoops. For example, however, the Para-Sail 80A is used without a center line, whereas many tests with Configuration IV were made with the arrangement of the center line. Furthermore, the profile of the plan form of the Para-Sail 80A and the Configuration IV are identical, but the 80A has 72 gores whereas Configuration IV has only 36 gores. However, for the purpose of model experiments, Configuration IV may be considered representing the Para-Sail 80A. It is schematically shown in Figs 11A and 11B.

Full size Para-Sails resembling this configuration have been tested and are called in the respective drop test report (Vol II) Para-Sail 80A-2 and 80A-3.

All models have a nominal diameter of approximately 4 ft or 2 ft when used for pendulum and free drop tests and three-component measurements, respectively. The models were built of light weight nylon with various nominal porosities.

Additional model configurations were used, with



RISER	RISER NO.	LINE LENGTH (INCLUDING RISER)
RIGHT FRONT	1—9	$1.00D_0$
LEFT FRONT	10—18	$1.00D_0$
RIGHT REAR	19—27	$1.00D_0$
LEFT REAR	28—36	$1.00D_0$

FIG 11 A. SCHEMATIC PLANFORM AND SUSPENSION LINE LENGTHS OF PARASAIL CONFIGURATION IV

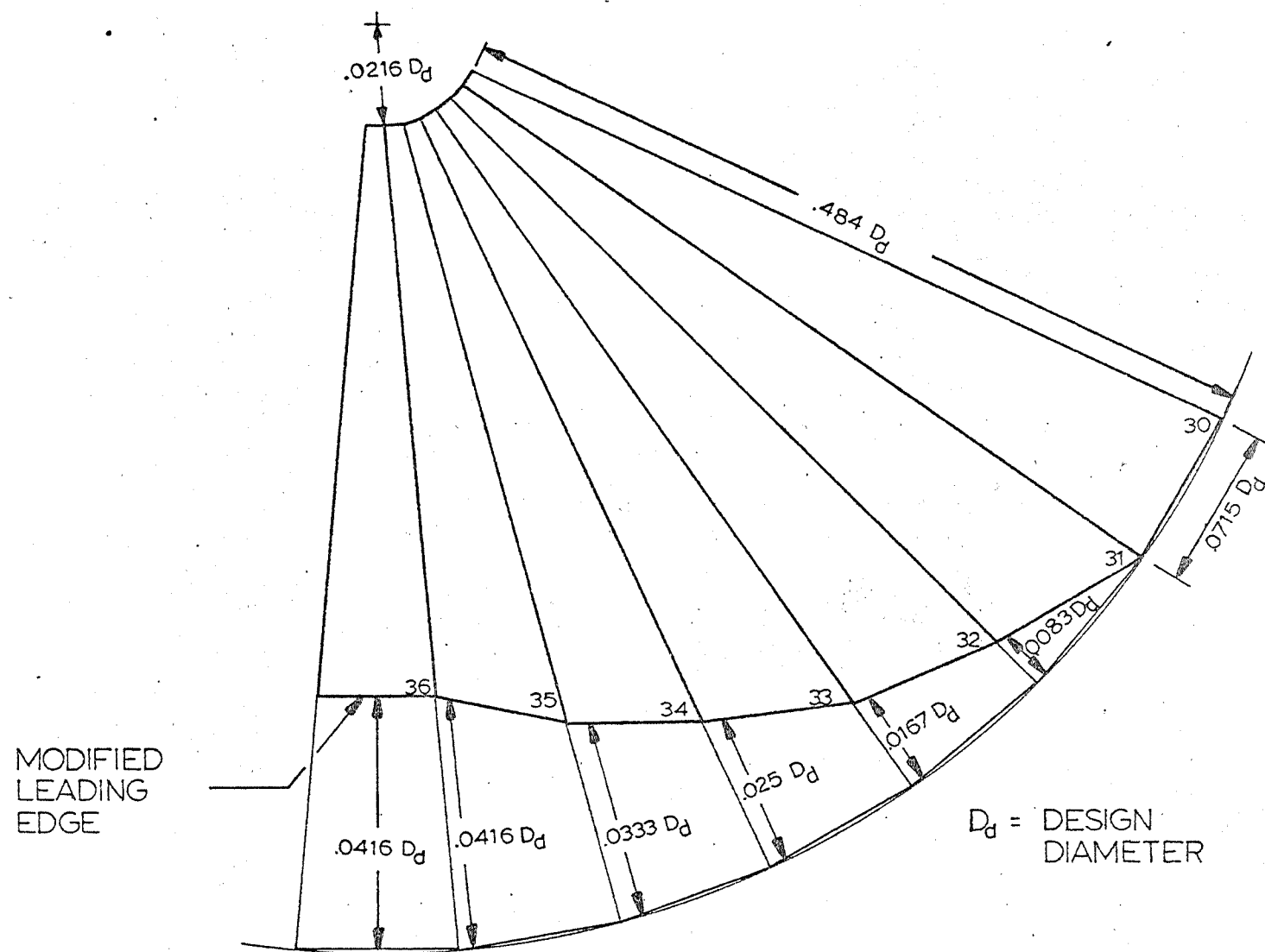


FIG 11 B. DIMENSIONLESS GORE PATTERNS FOR SOLID FRONT PANELS OF CONFIGURATION IV

the purpose of exploring the effects of an internal parachute,  
of the center line and other more operational objectives  
and problems.

### III. NOTATION

Since many terms needed in the discussion of a gliding parachute had to be originally established, an attempt will be made to describe and justify these novel terms.

In order to identify the models with respect to size, porosity and configuration, the following symbolism will be employed. The configuration number will come first, then the design diameter of the parachute (in inches), and finally the nominal porosity of the parachute cloth (in units of  $\text{ft}^3/\text{ft}^2\text{-min}$ ). For example, I-48-4.67 defines Configuration I, having a 48" design diameter and a nominal porosity of  $4.67 \text{ ft}^3/\text{ft}^2\text{-min}$ .

Several design characteristics of more specific nature are illustrated in Figs 12, 13 and 14. For example, the center line, which connects the apex of the canopy with the risers, is shown in Fig 13. The numbering of the canopy gores is illustrated in Fig 14.

Attempting to describe the aerodynamic characteristics of a gliding parachute such as the Para-Sail, it is convenient to use a system of coordinates and stability notation as shown in Fig 15, which is a combination of the coordinate systems used in parachute and aircraft technology. This system allows the description of the performance characteristics such as the angle of attack,  $\alpha$ , the longitudinal stability or pitch, the lateral stability or roll, and the yaw stability. Pitch, roll and yaw are expressed as an

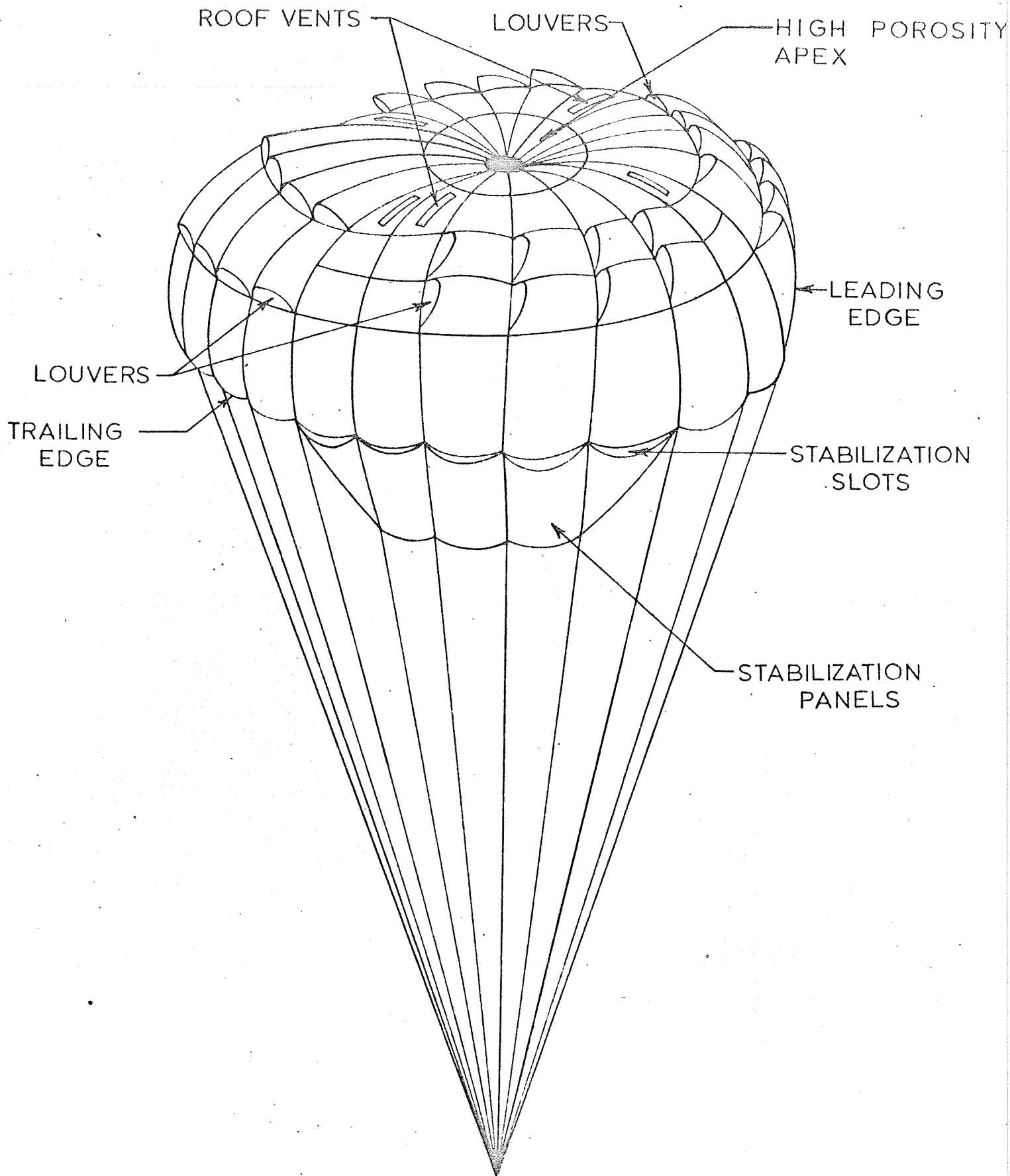


FIG 12. PARASAIL NOMENCLATURE

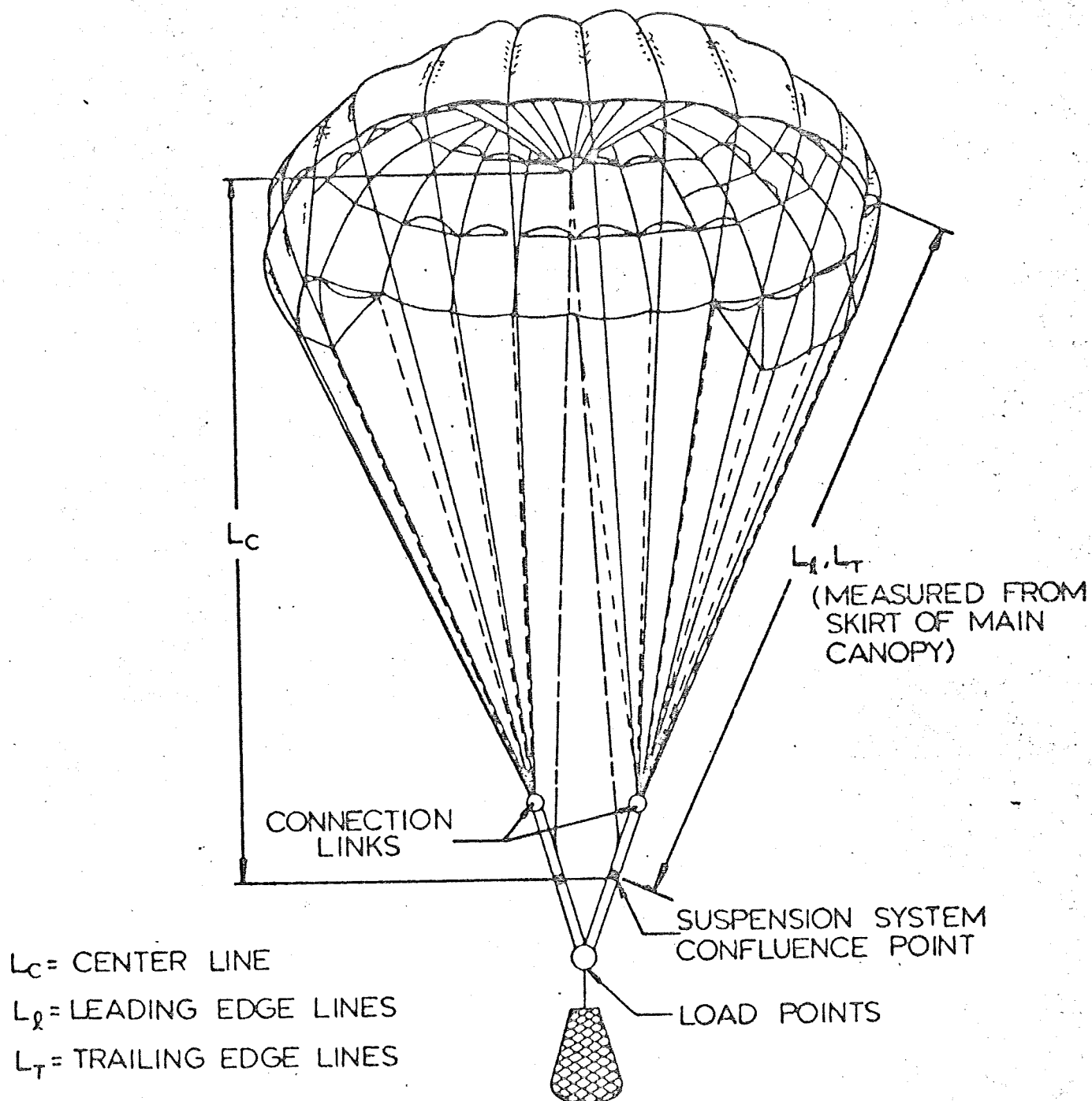


FIG 14. LOCATION OF LINES FOR PARASAIL

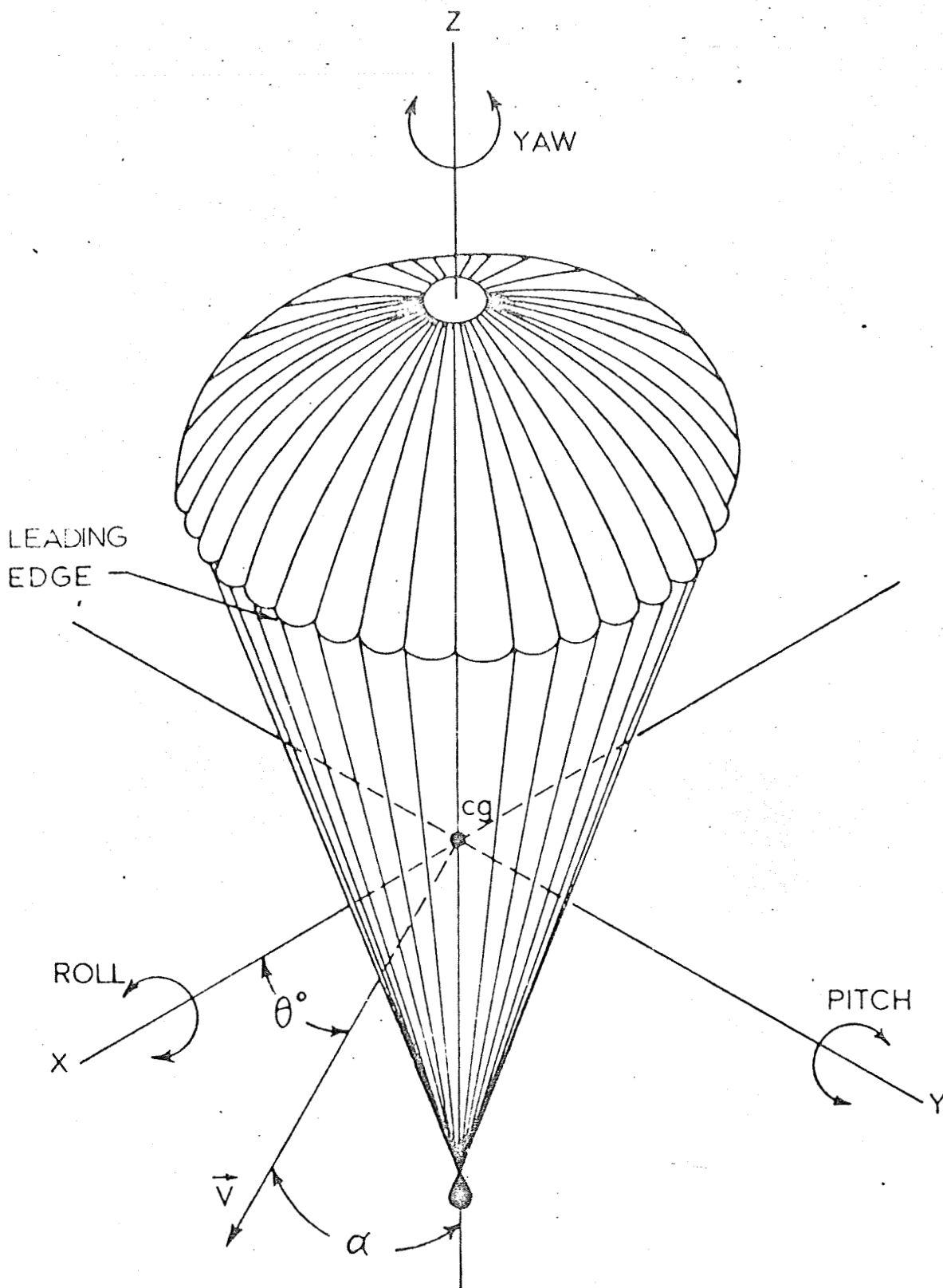


FIG. 15. STABILITY NOTATION FOR GLIDING PARACHUTE

angular deviation from the mean stable position. Thus, a parachute which has a small angular deviation from its mean, or average position would be termed stable about its three principal axes.

#### IV. CONFIGURATION I

The efforts under this section can be organized into an attempt to establish the aerodynamic characteristics of a parachute with a canopy plan form as shown in Fig 4, and to modify this plan form as well as the suspension line arrangement in order to obtain an L/D ratio higher than that displayed by the original form.

Pertinent, exploratory tests and modifications were made which gradually led to Configuration II (Fig 5). The more complete examinations of this configuration, however, are described in the next section entitled "Configuration II."

##### A. Investigation of Original Para-Sail

###### Flow Studies

The first step in this investigation was the exploration of the flow field on the surface of the Para-Sail canopy. This was accomplished by placing small tufts on the outside surface and observing their placement due to the air flow around the immersed canopy. A graphical representation of the results is shown in Fig 16. In general, the flow pattern has the expected form, but of interest is the large area of turbulence near the vent and on the upper downstream side.

###### Stable Angle of Attack--L/D Ratio

Secondly, information on the stable angle of attack and its variation with porosity was obtained. The stable angle of attack,  $\alpha$ , or stable angle as it will hereafter be called, was measured at velocities of 20 through 40 ft/sec on

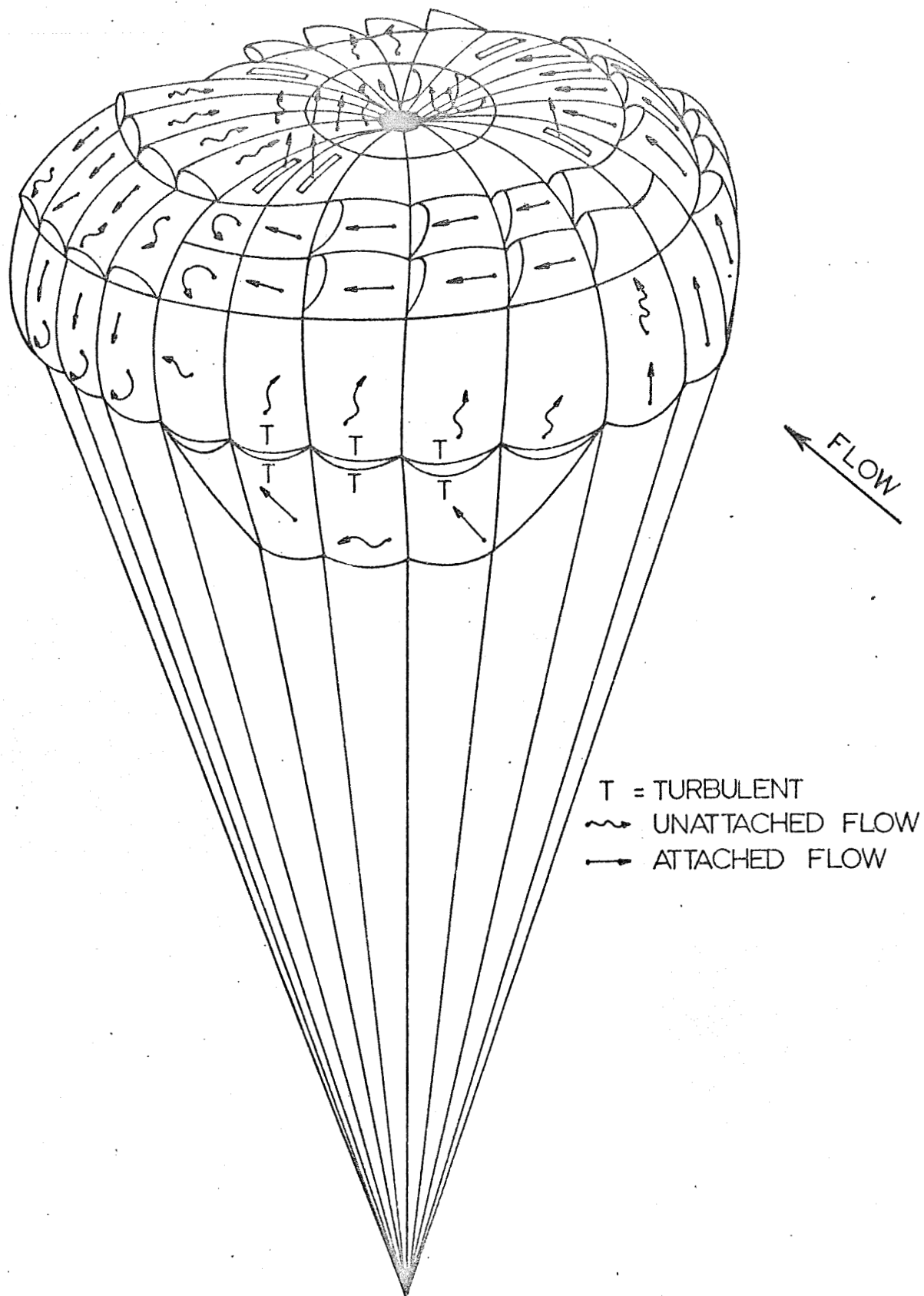


FIG. 16. FLOW FIELD ABOUT PARASAIL

32" diameter models having nominal porosities of 4.67, 47 and 105 ft<sup>3</sup>/ft<sup>2</sup>-min.

For these studies, the models were first suspended from an angular measuring device which has free motion in the vertical plane. A schematic representation of this system for so-called pendulum tests is shown in Fig 17. A close-up of the pendulum device is shown in Fig 18. The angle of attack was determined by measuring the change in a variable resistance element mounted in the pendulum device. The electrical output was recorded on photographic paper by means of a Century Oscillograph. Figure 19 shows the pendulum testing arrangement and the recording equipment. An example of an experimental record is shown in Fig 20 from which the stable angle of attack and the pitch stability can be measured. Roll and yaw stability were determined by visual observation.

The results of these experiments are shown in Fig 21. It can be seen that the stable angle of attack and also the L/D ratio decreased with increasing velocity. This was particularly pronounced in models with higher porosity.

The decrease of the stable angle with increasing porosity, at any given speed or canopy loading, is a known fact (Ref 1). However, the decrease of the stable angle with increasing velocity or higher canopy loading cannot be explained at this time.

On the other hand, for equal canopy loadings, one may expect an increase of canopy lift with increasing canopy size due to a Reynolds number effect as known from airfoils.

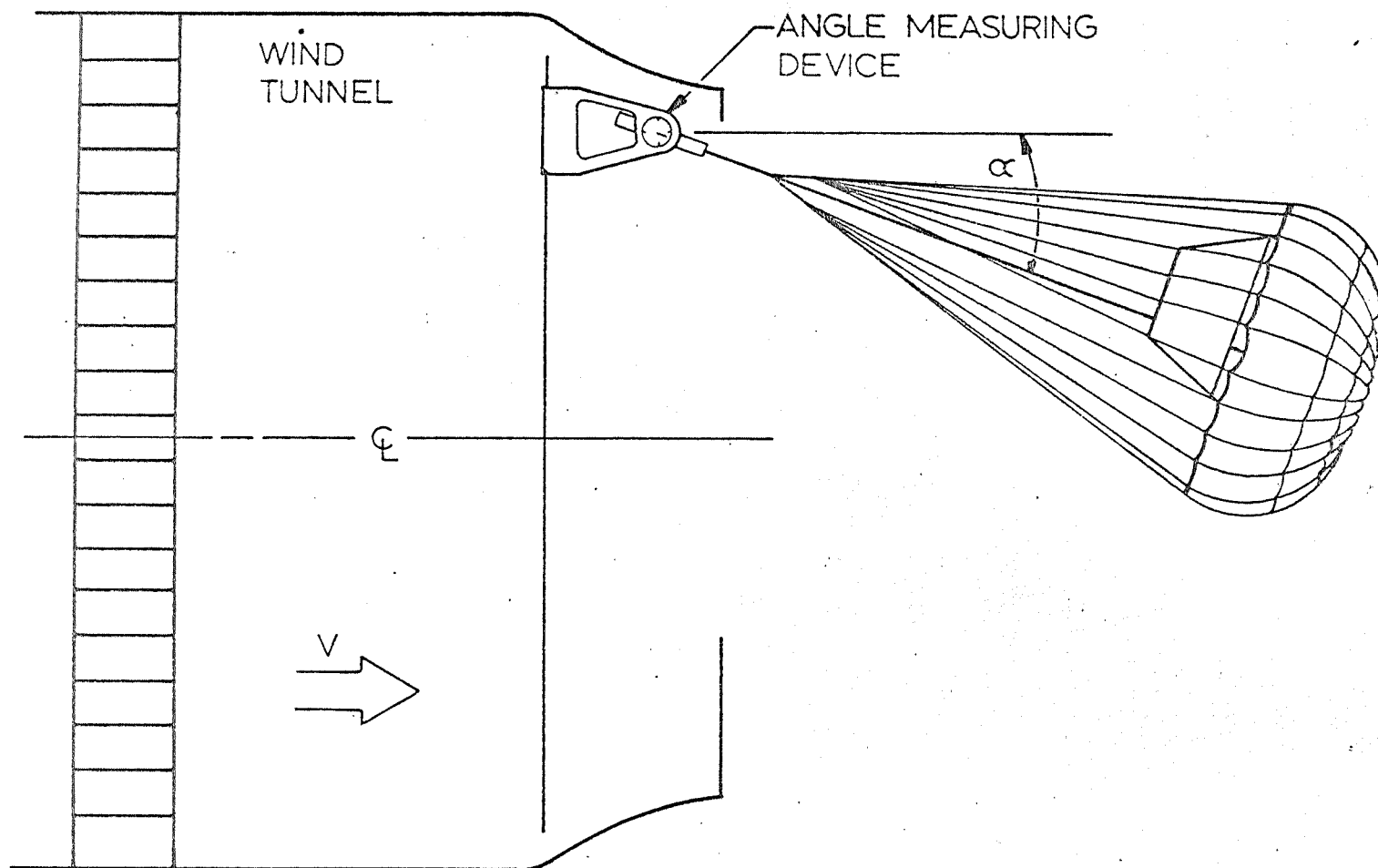
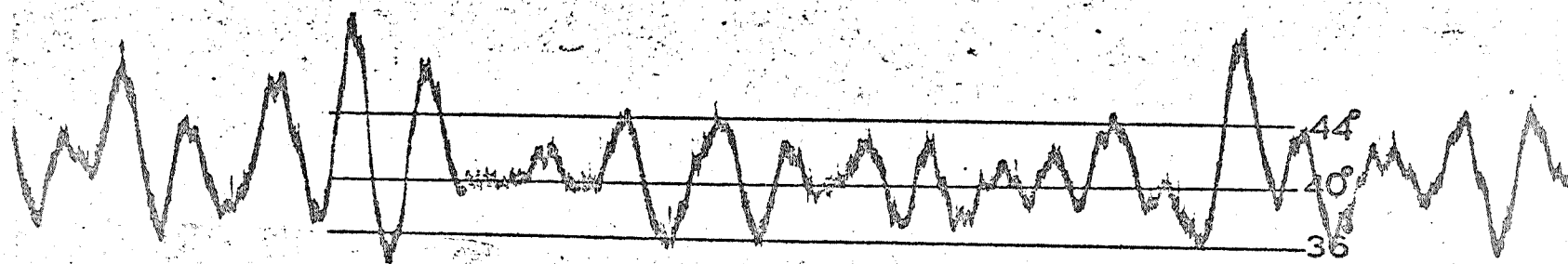


FIG 17. SUBSONIC WIND TUNNEL TEST ARRANGEMENT  
FOR PENDULUM TESTS



PARA-SAIL

MODEL - Configuration I

DATE - 1/28/63

VELOCITY - 25 fps

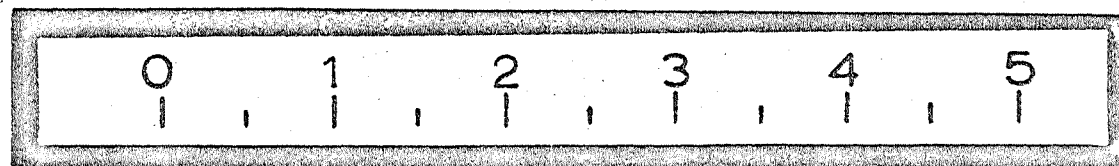


FIG. 20. TYPICAL OSCILLOGRAPH RECORDING OF MOTION OF A PARACHUTE IN PENDULUM TESTS

This would mean that large Para-Sails, say on the order of 80 ft nominal diameter, would have a higher L/D ratio or a larger stable angle than the respective Para-Sail model. In view of this consideration, the stable angles indicated in Fig 21 should be considered as the lower limits of larger Para-Sails.

In summary, a large Para-Sail, Configuration I, having a low nominal porosity should have a minimum L/D ratio of at least 0.84 at a rate of descent of approximately 25 ft/sec.

#### L/D Ratio and Line Adjustments

Further studies were conducted to see the effect of line length changes on the stable angle. These tests showed that shortening or lengthening the center line did not appreciably change the stable angle, although after the center line was shortened beyond a critical point, the canopy would collapse.

Also complete removal of the center line did not effectively change the stable angle.

However, changes in the length of the risers did produce a considerable variation in the stable angle. In fact, by adjusting the risers to different lengths, a variation of the stable angle from  $30^{\circ}$  to  $43^{\circ}$  was observed. In these experiments, the front riser lengths were adjusted with respect to the rear risers, which length were kept constant. In all cases, an increase in the length of the front risers

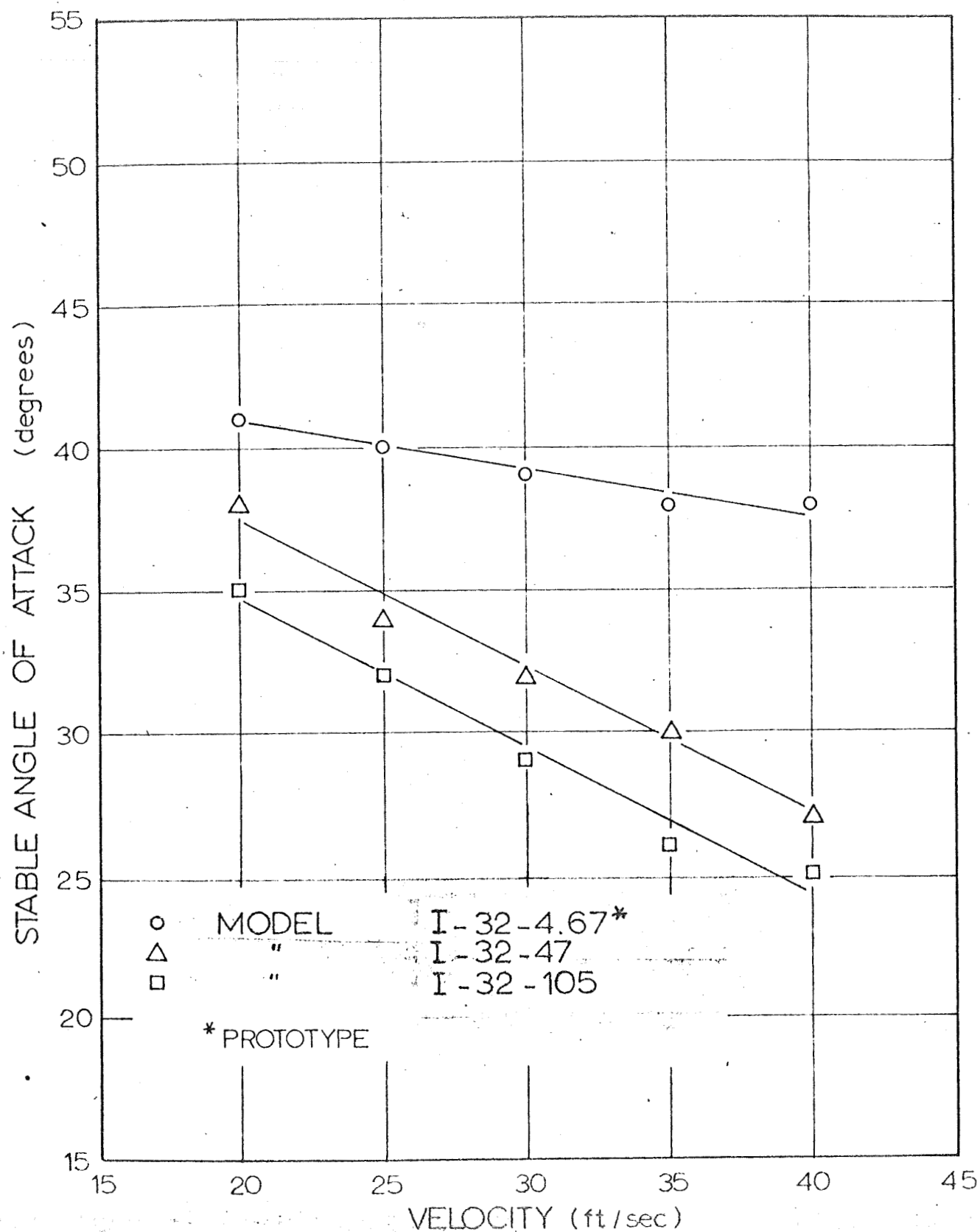


FIG 21. STABLE ANGLE OF ATTACK vs VELOCITY FOR CONFIGURATION I WITH VARIOUS NOMINAL POROSITIES

produced a decrease in the stable angle and a decrease in the front riser lengths produced up to a critical point an increase in the stable angle. Details will be presented later on in this section when the three-component studies are discussed (Fig 28 and Table 1).

#### Effect of Slots and Louvers

The slots and louvers were opened and closed symmetrically to determine their effect on the stable angle. For these tests Model I-32-4.67 was used.

With all the slots and louvers closed, the stable angle was measured and found to be approximately  $30^{\circ}$ . As the slots and louvers were opened methodically, the stable angle increased until all slots and louvers were opened. At this point the stable angle was found to be  $40^{\circ}$ . Therefore, it may be concluded that for the basic Configuration I, the arrangement of the slots and louvers represents an optimum solution.

#### Three-Component Measurements

It should be remembered that for all the angle measurements made in the studies presented above, the pendulum method was employed, since only the study's general trends were desired. After completion of this objective, three-component measurements were made to more accurately determine the stable angle as well as the inherent stability of the parachute when deflected from its stable position. Figure 22 shows Configuration I arranged on the three-component balance system. Figures 23 through 30 present the results of the three-component measurements.

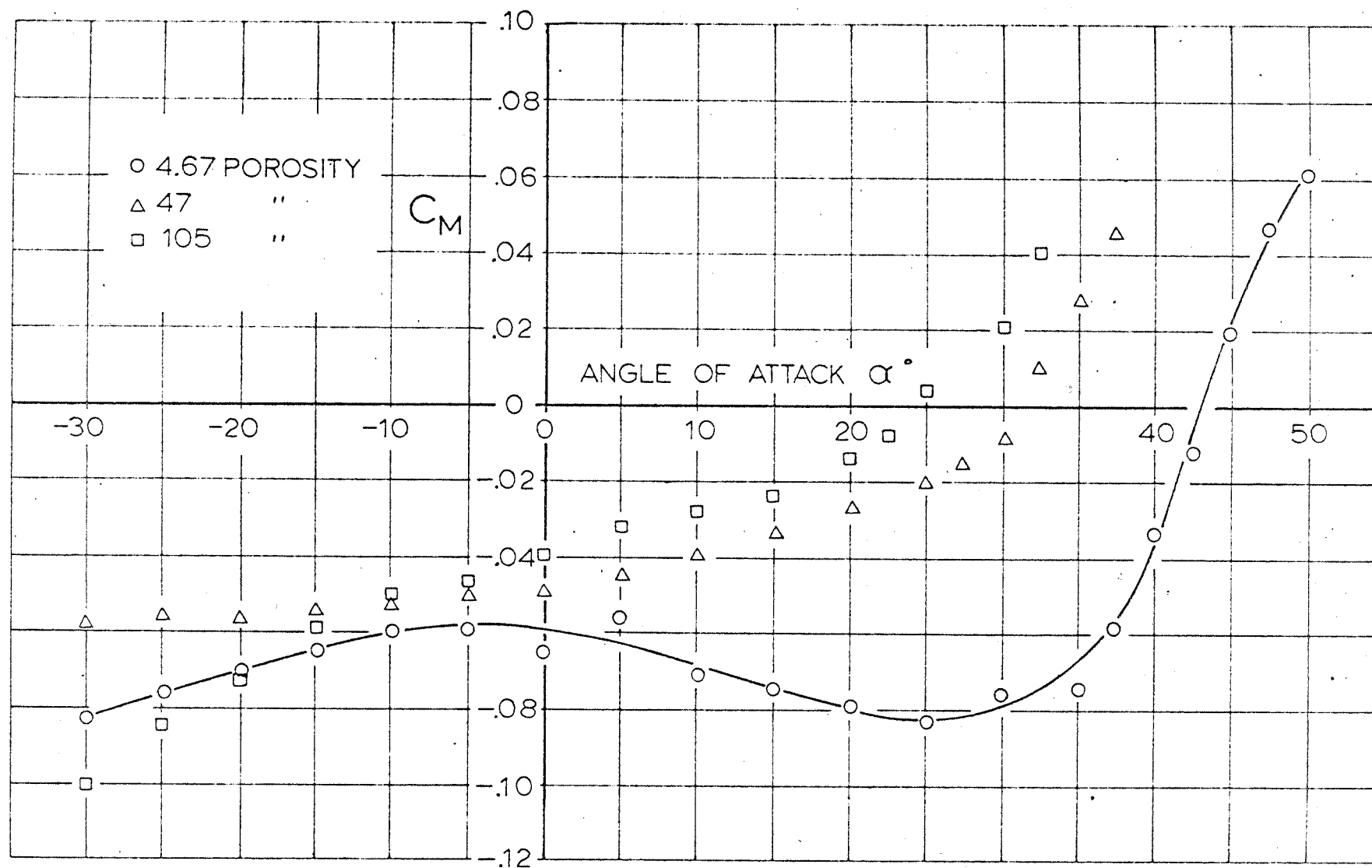


FIG. 23. MOMENT COEFFICIENT VS. ANGLE OF ATTACK  
FOR CONFIGURATION I

(BASED ON TOTAL SURFACE AREA  $S_o$ , REYNOLDS NUMBER =  $8 \times 10^5$ ;  $D_o = 24"$ )

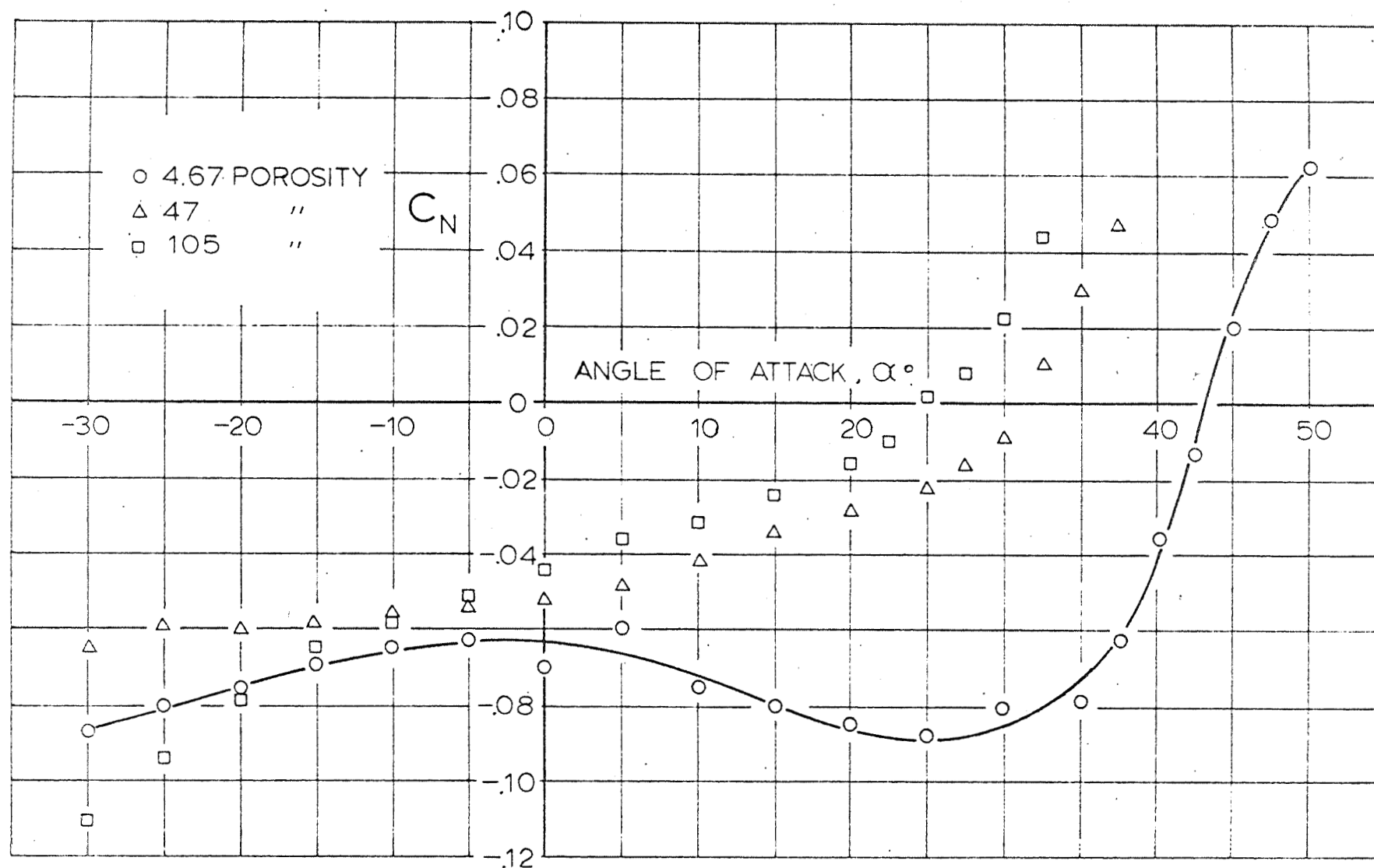


FIG. 24. NORMAL FORCE COEFFICIENT VS. ANGLE OF ATTACK FOR CONFIGURATION I

(BASED ON TOTAL SURFACE AREA  $S_o$ , REYNOLDS NUMBER =  $8 \times 10^5$ ;  $D_o = 24"$ )

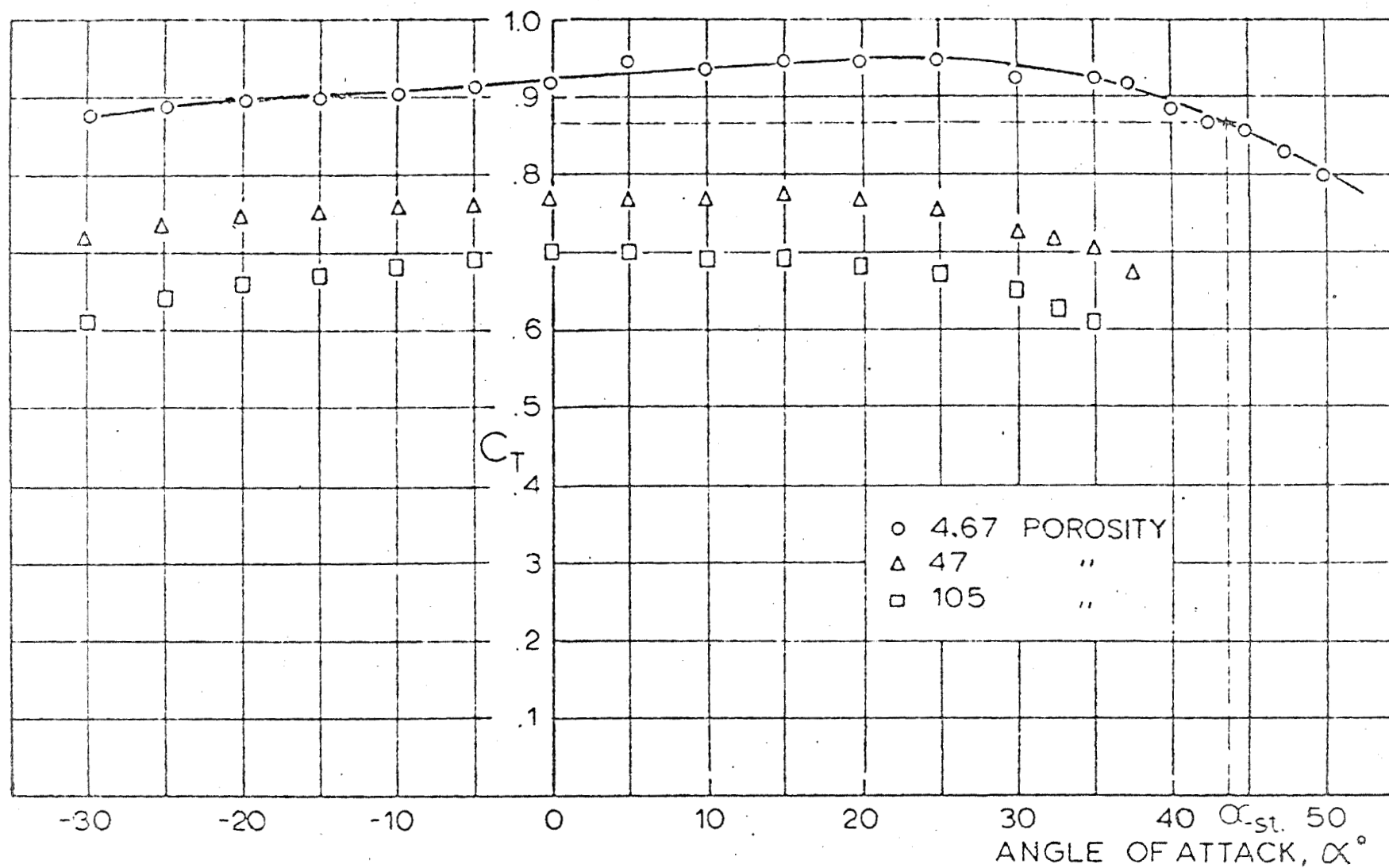


FIG 25. TANGENT FORCE COEFFICIENT VS ANGLE OF ATTACK FOR CONFIGURATION I

(BASED ON TOTAL SURFACE AREA  $S_0$ ; REYNOLDS NUMBER =  $8 \times 10^5$ ;  $D_0 = 24'$ )

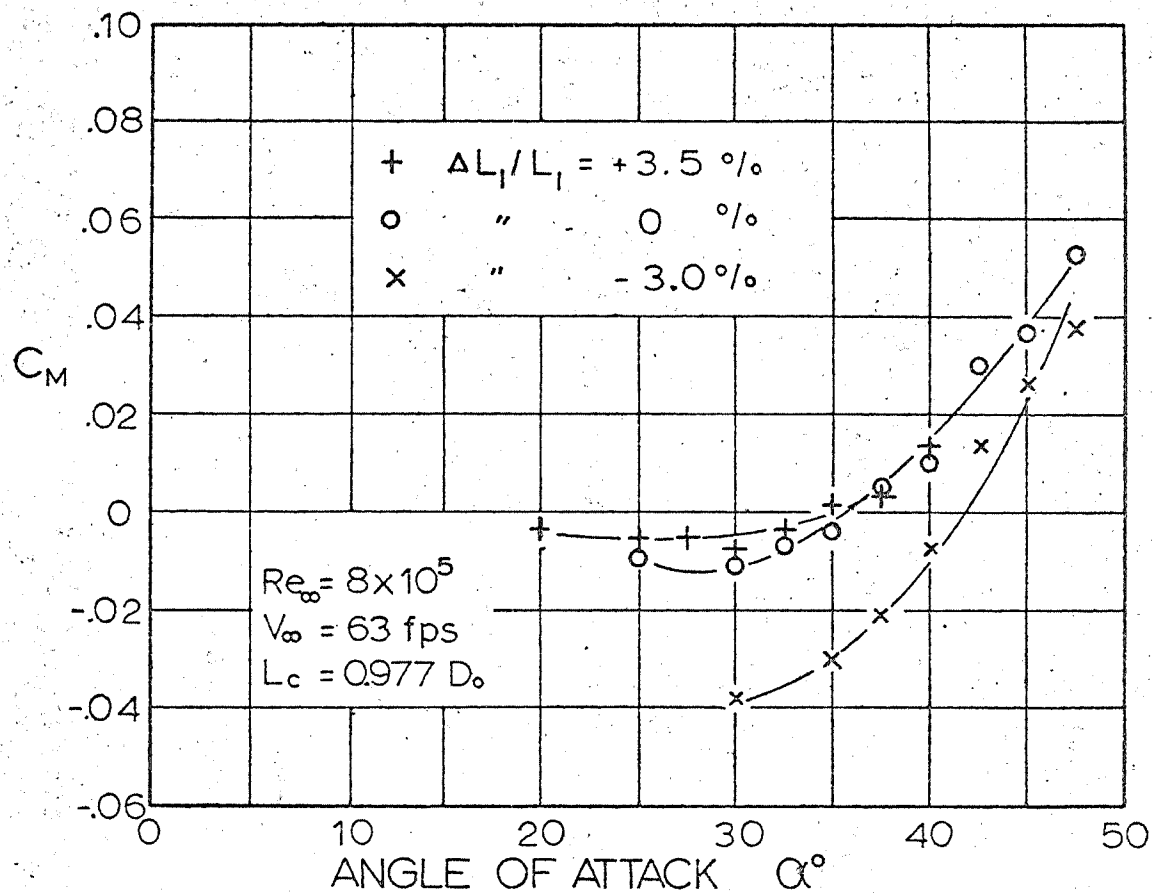


FIG 26. MOMENT COEFFICIENT vs ANGLE OF ATTACK FOR MODEL I-24-4.67 WITH VARIATIONS IN THE FRONT RISER LENGTHS (BASED ON TOTAL SURFACE AREA  $S_o$ )

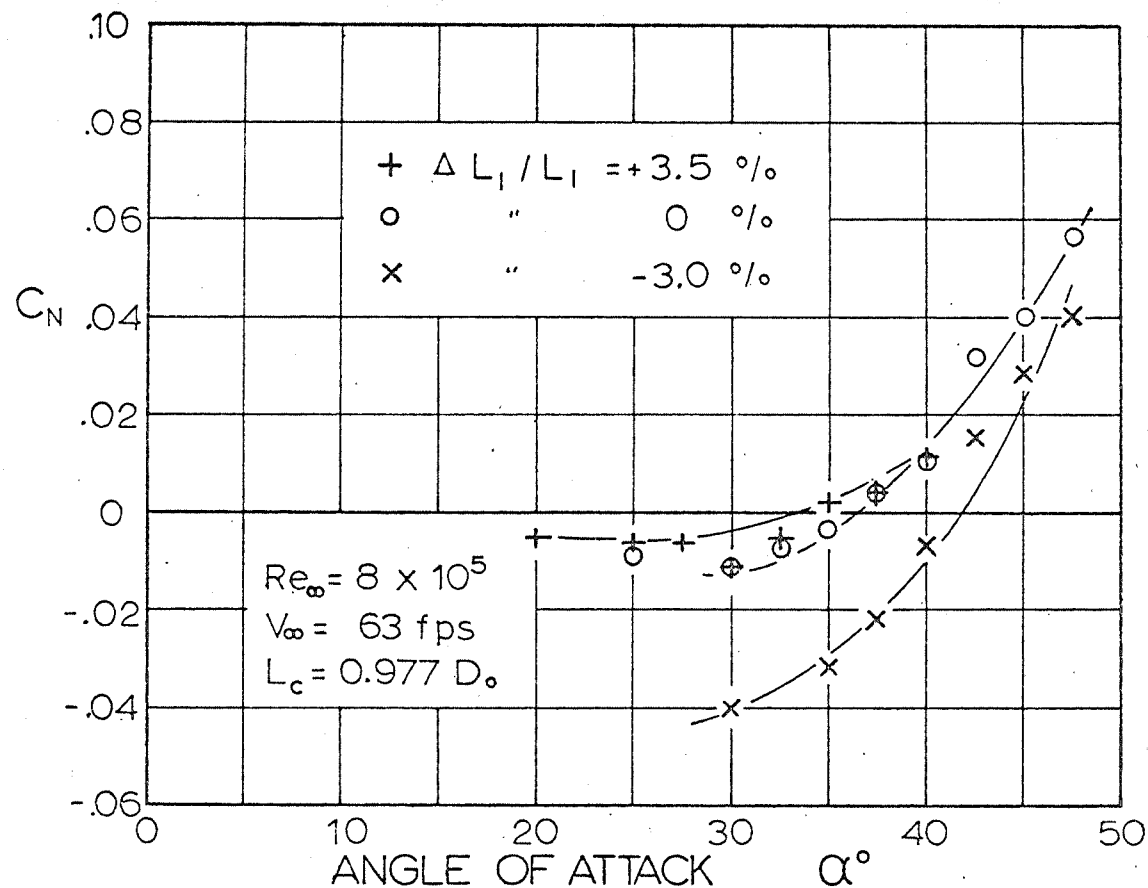


FIG 27. NORMAL FORCE COEFFICIENT vs ANGLE OF ATTACK FOR MODEL I - 24 - 4.67 WITH VARIATIONS IN FRONT RISER LENGTHS (COEFFICIENTS BASED ON TOTAL SURFACE AREA,  $S_o$ )

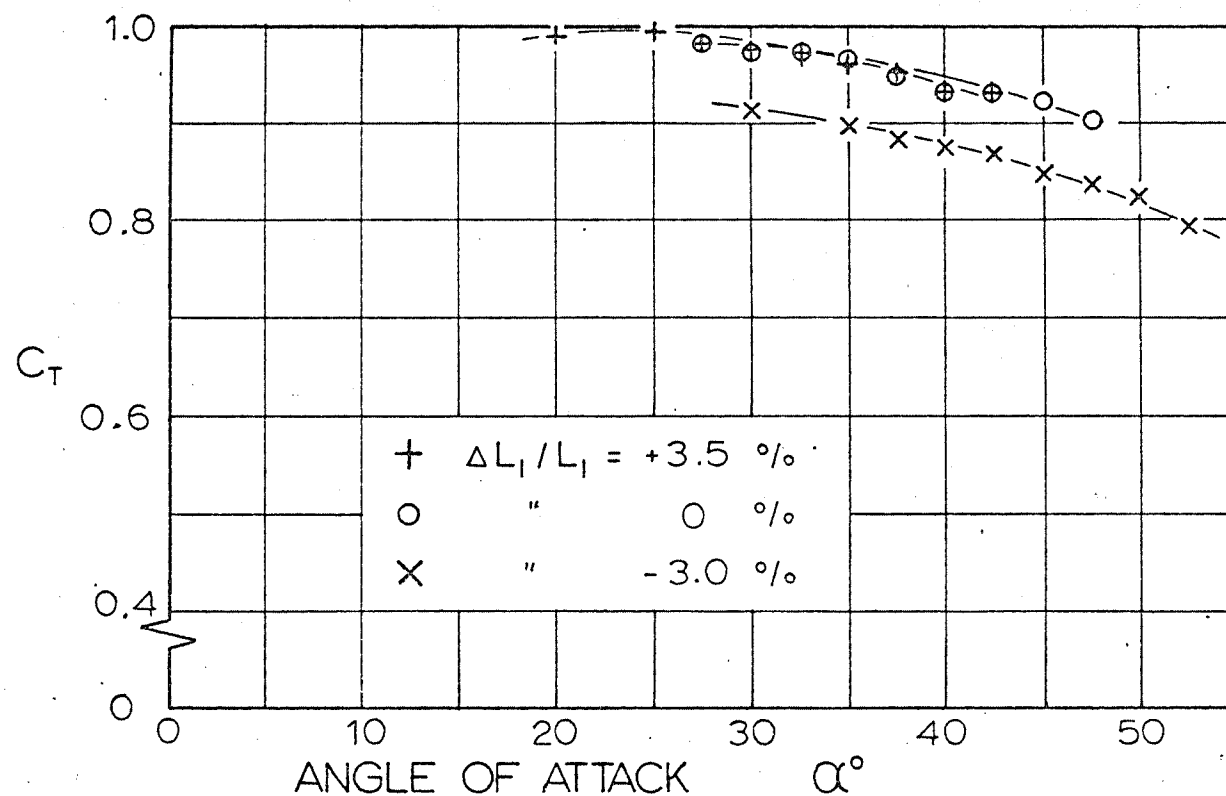


FIG 28. TANGENT FORCE COEFFICIENT vs ANGLE OF ATTACK FOR MODEL I-24-4.67 WITH VARIATIONS IN THE FRONT RISER LENGTH (COEFFICIENTS BASED ON TOTAL SURFACE AREA,  $S_o$ )

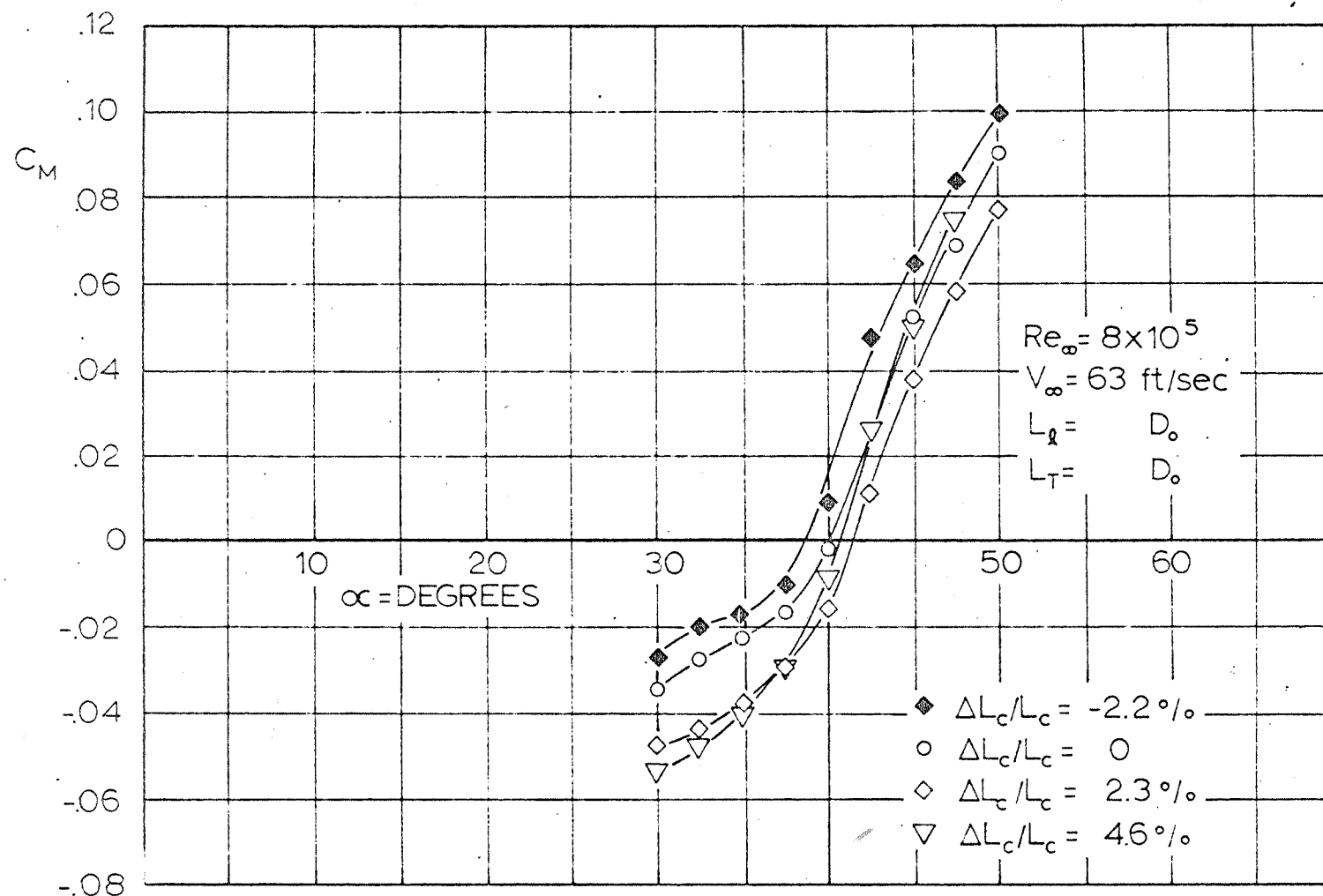


FIG 29. MOMENT COEFFICIENT vs ANGLE OF ATTACK FOR MODEL I-24-467 WITH VARIATION IN THE CENTER LINE LENGTH (COEFFICIENTS BASED ON TOTAL CLOTH AREA  $S_o$ .)

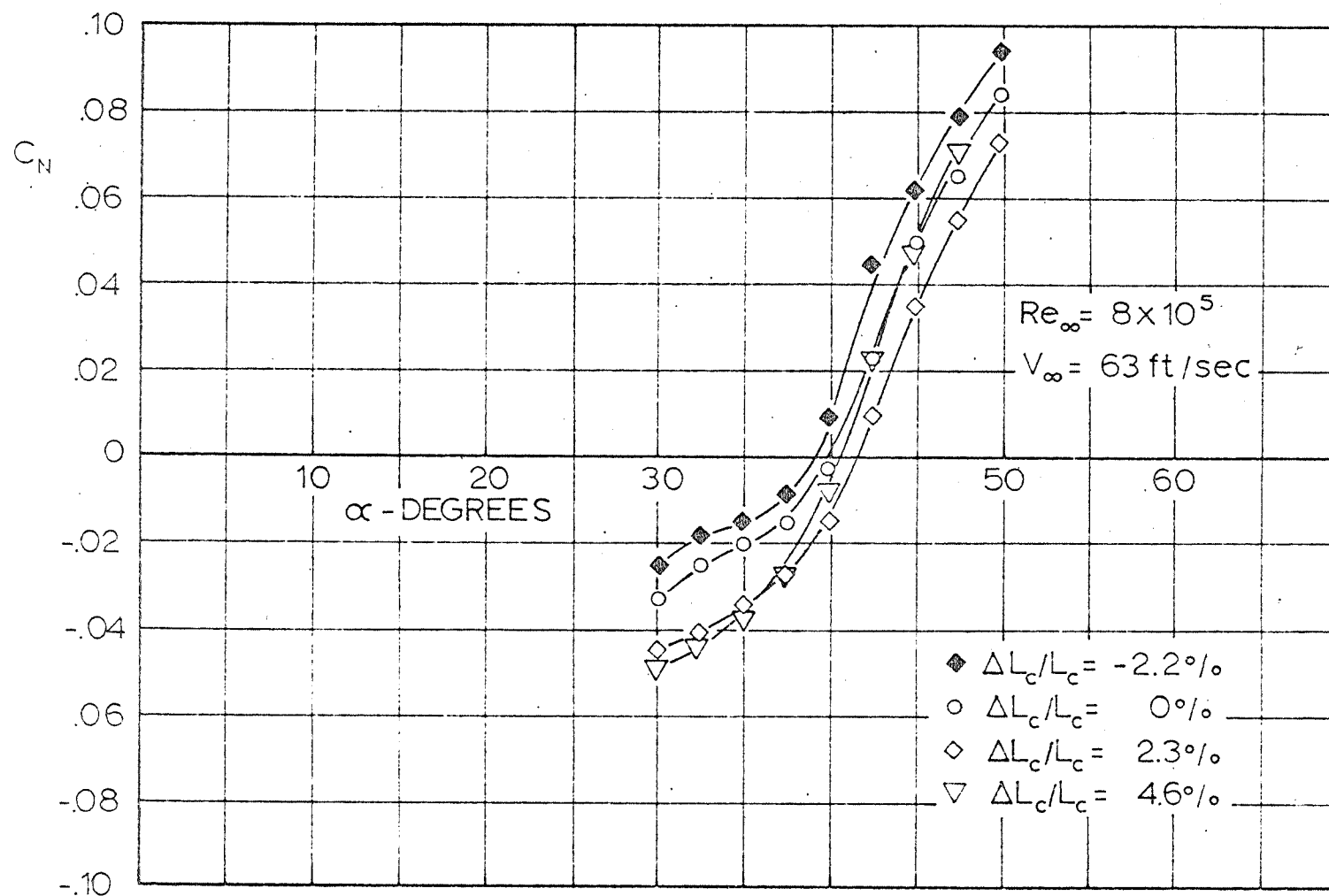


FIG 30. NORMAL FORCE COEFFICIENT vs ANGLE OF ATTACK FOR MODEL I-24-4.67 WITH VARIATION IN THE CENTERLINE LENGTH (COEFFICIENTS BASED ON TOTAL CLOTH AREA  $S_o$ .)

The procedure for the three-component tests is described in detail in Ref 1. A schematic of the suspension system used for these studies is shown in Figs 31 and 32. Figure 32 shows the location of the strain gage elements used to measure the forces on the canopy. Again, this was accomplished by feeding the electrical output into a Century Oscillograph and its recording mechanism.

The forces measured during these tests and used to determine the aerodynamic coefficients are defined in Fig 33. The tangent force, T, acts along the centerline of the canopy, while the normal force, N, acts perpendicular to the center line of the canopy and produces the aerodynamic moment, M, about the confluence point of the suspension lines.\* From these measured forces, the aerodynamic coefficients can be calculated using the conventional aerodynamic relationships (Ref 2, Parachute Handbook), where

$$C_T = \frac{T}{qS} \quad (1)$$

$$C_N = \frac{N}{qS} \quad (2)$$

and

$$C_M = \frac{M}{qSD} \quad (3)$$

\*This is merely an approximation, but a satisfactory one, see Ref. 1.

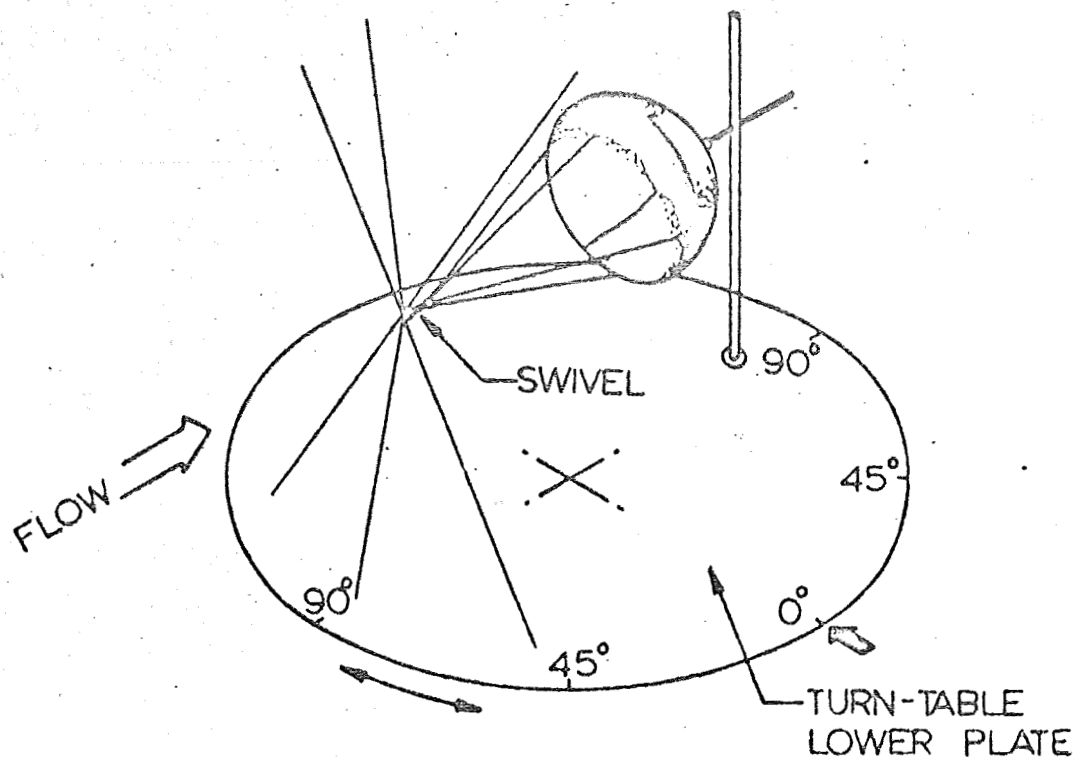


FIG 31. MODEL SUSPENSION FOR MEASURING NORMAL FORCE AND TANGENT FORCE

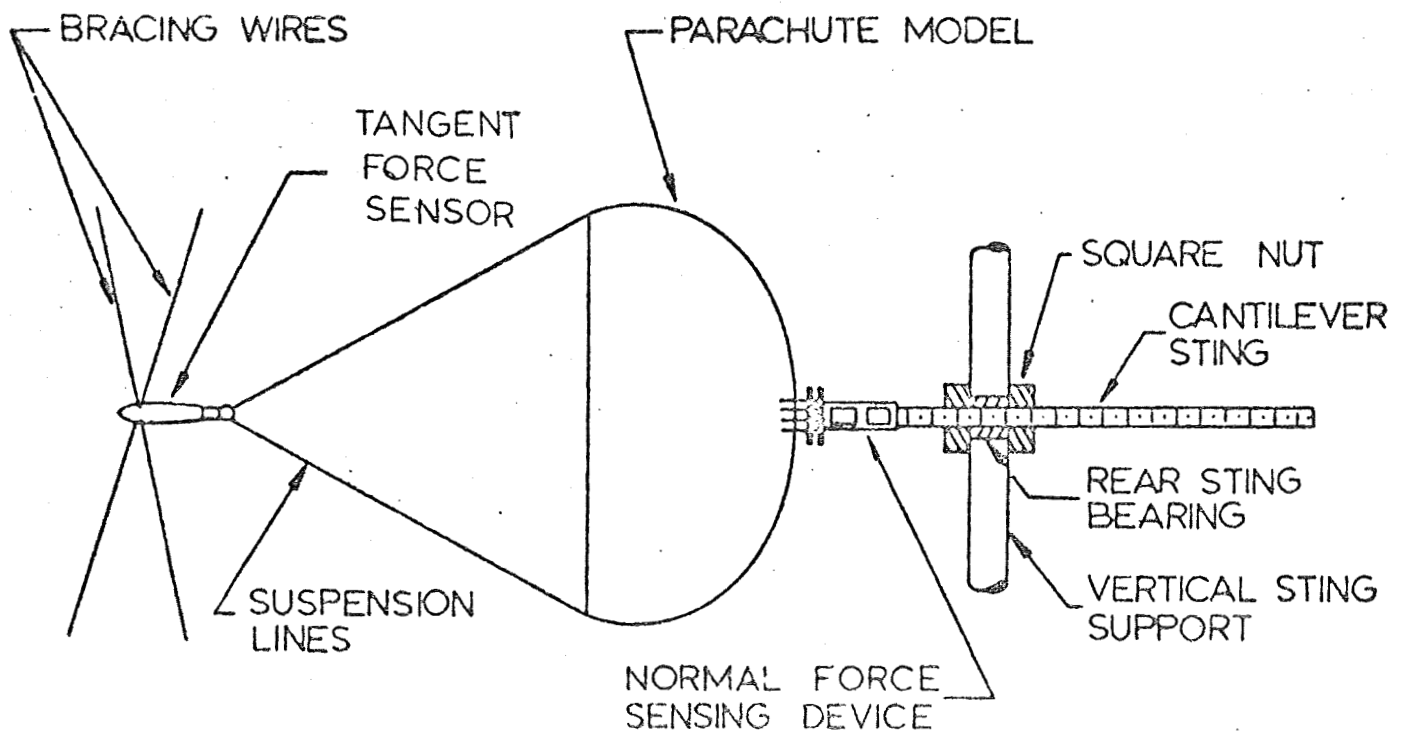


FIG 32. MODEL SUSPENSION AND STRAIN GAGE BALANCE ARRANGEMENT FOR MEASURING NORMAL FORCE AND TANGENT FORCE

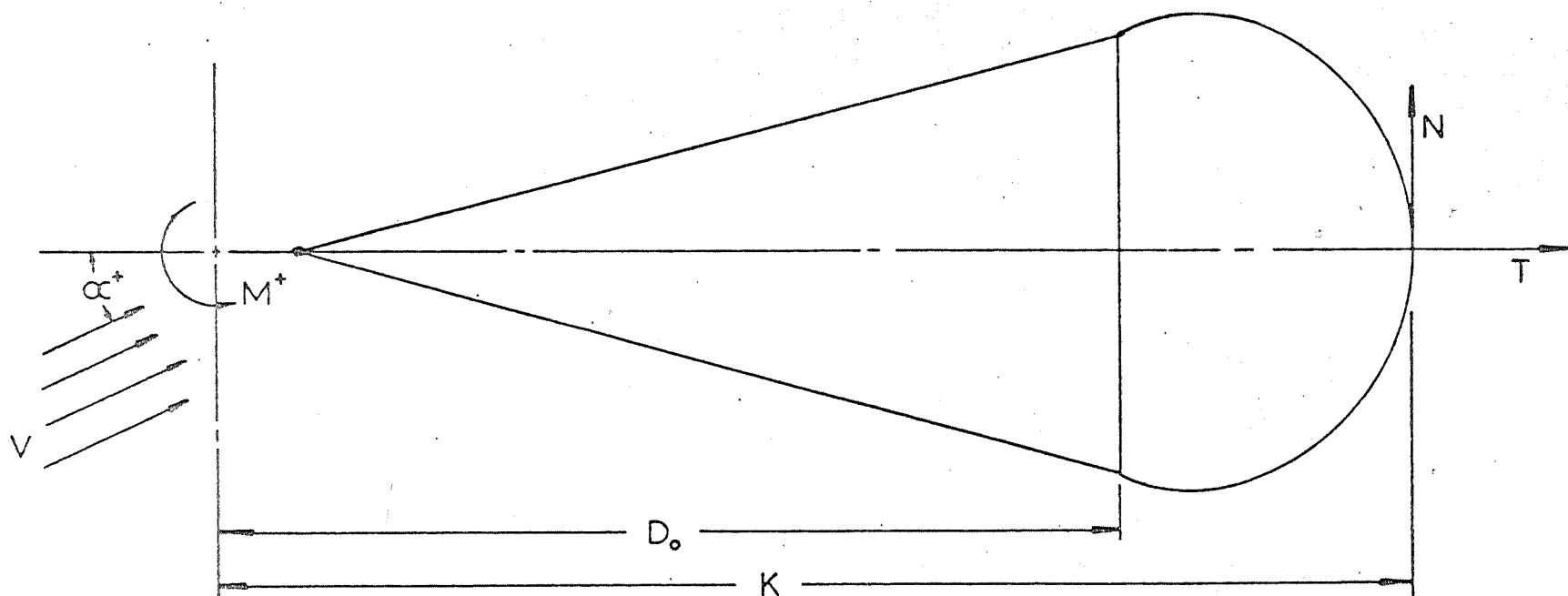


FIG. 33. FORCES AND COORDINATES USED FOR DETERMINING AERODYNAMIC COEFFICIENTS

Thus, a stable position will exist when

$$M = 0 \quad (4)$$

and

$$\left. \frac{\partial C_M}{\partial \alpha} \right|_{M=0} > 0 \quad (5)$$

In particular, Figs. 23 through 25 show the variation of the stable angle with porosity while holding the velocity and the line lengths constant. Figures 26 through 28 show the variation in the stable angle as a function of the front riser length. The low porosity Model I-24-4.67 was used for these tests, since it was apparent from previous studies that the low porosity model displayed the largest glide angle. Finally, Figs 29 and 30 present the variation in the stable angle as the center line length is changed. Again, Model I-24-4.67 was used for the tests.

Whereas the figures indicate details of the various effects and operational characteristics, the principal results are summarized in the following conclusions.

- 1) Increasing the nominal porosity of the parachute tends to decrease the glide angle.
- 2) Changing the length of the front risers, affects noticeably the stable angle or the L/D ratio. Decreasing the length of the front risers with respect to the back risers, the stable angle increases until a maximum is reached, whereupon a further decrease tends to decrease the stable

angle. Numerical values have been obtained, which indicate a possible lift to drag modulation.

- 3) Moderate changes in the center line length or its complete removal do not appreciably change the stable angle of the parachute.
- 4) All the models tested are stable at only one angle of attack.
- 5) The low porosity models have a greater value of  $dC_M/d\alpha$  than the models with higher porosity. Thus, the low porosity models will assume their stable angle of attack more rapidly and have less oscillation about that angle than the high porosity models.
- 6) All models have a relatively high value of  $C_T$  at the stable angle and consequently should operate with a relatively low rate of descent.

The stable angles measured in the three-component studies are somewhat higher than the values obtained from the pendulum tests. This can possibly be explained by the fact that relatively large models were used for the three-component measurements and at high angles of attack the canopy skirt came within one diameter of the tunnel wall. Thus, wind tunnel interferences may have affected the parachute at larger angles of attack. It is suggested that the results of the pendulum tests be considered to be the lower limit of the stable angle of attack.

### Line Forces

After the three-component tests were completed, the forces in the individual risers were measured in an attempt to determine the forces necessary to achieve a lift-drag modulation.

In these tests the models were suspended from the angular indicator used in the pendulum tests. Electric force sensing elements were then placed in the risers as shown in Fig. 34 and their output was recorded by means of Century Oscillograph.

The total forces measured in the risers and center lines during these tests should equal the tangent force at  $\alpha_{\text{stable}}$  determined from the three-component tests. This has been verified from the experimental results.

The forces in the front risers, center lines, and the rear risers, divided by the total force of the parachute are given in Table I. One notices that in the middle position  $\Delta L_l/L_l = 0$ , and the front risers, rear risers and center lines carry approximately one third of the total force. However, a major portion of the force shifts to the front risers when a stable angle is increased or toward the rear risers as the angle of attack decreases.

All models used for these line tension tests had six suspension lines connected to each one of the four risers.

However, since full size drop tests were made in which the front risers carried five suspension lines while six lines were connected to the rear risers, a configuration with the so-called 5 x 7 line connection was also tested.

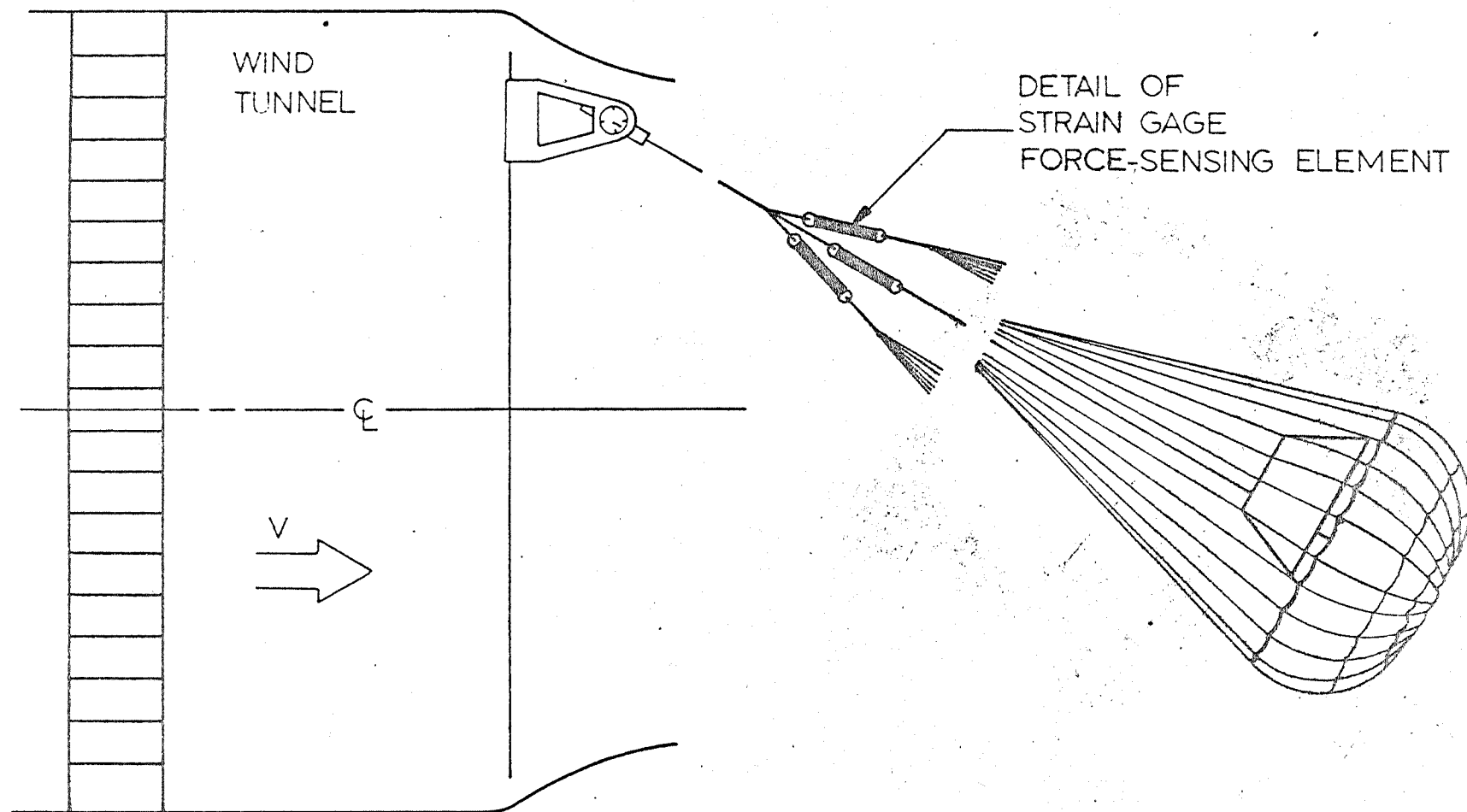


FIG 34. SUBSONIC WIND TUNNEL TEST ARRANGEMENT  
FOR LINE TENSION TESTS

TABLE I. RATIO OF LINE FORCE TO TOTAL FORCE FOR MODEL I-32-4.67 WITH DIFFERENT FRONT RISER LENGTHS

$\alpha_{st}^\circ$	$C_{T0}$	Front Riser Adjustment $\Delta L_\ell / L_\ell$ (3)	Per Cent of Total Force		
			Front Risers (1)	Center Line	Rear Risers (2)
30°	1.05	+0.035	29.6	34.0	37.9
37°	1.05	0.000	30.4	33.6	35.1
43°	0.88	-0.030	36.2	29.9	32.6

(1) Right front riser lines (1 - 6)  
Left front riser lines (19 - 24)

(2) Right rear riser lines (7 - 12)  
Left rear riser lines (13 - 18)

(3)  $\Delta L_\ell / L_\ell$  = Ratio; change in front line length to total line length ( $L_\ell = D_d$  for prototype Para-Sail).

Figure 35 gives a schematic view of Configuration I with a 5 x 7 line configuration. The results of these tests are presented below.

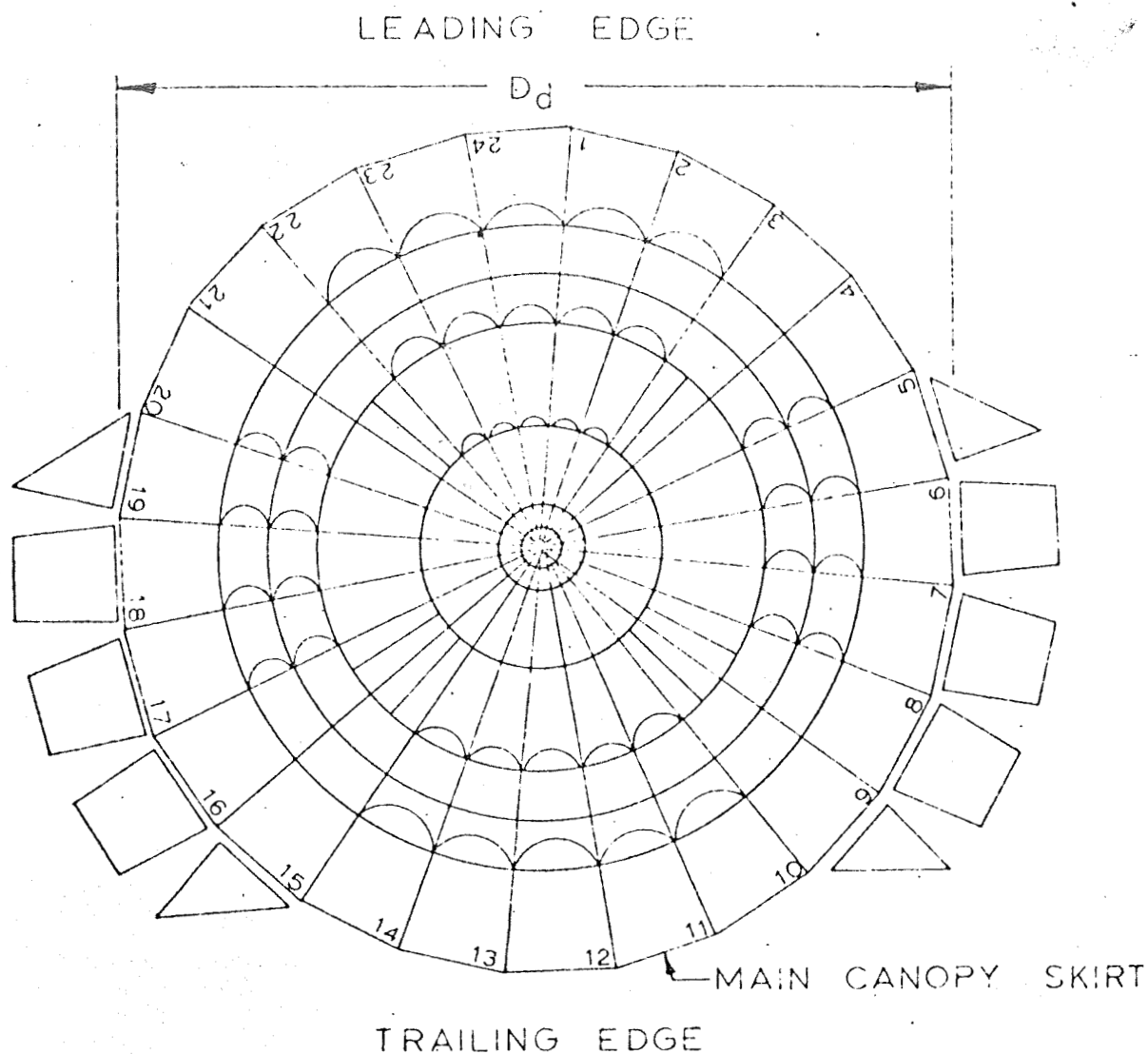
$\alpha$	Line Configuration	$C_{T_0}$	Front Riser Adjustment	Per Cent of Total Force		
				Front Riser	$C_L$	Rear Riser
37°	5x7	1.05	0.00	21.5	35.6	42.8

#### Center of Pressure

Finally, the aerodynamic center line of Configuration I was determined using Model I-32-4.67 with the basic 6 x 6 line configuration. This was accomplished in the following manner. Photographs were taken of the side view of the inflated parachute. From these photographs the directions in which the riser forces act was obtained. Knowing the direction and the magnitude of the riser forces, the resultant force, its direction in particular, can be obtained. Since the line of action goes through the center of pressure, its location with respect to the canopy is thereby determined. Figure 36 illustrates the described conditions.

#### B. Modification of the Para-Sail Configuration I

Once the stable angle and other aerodynamic characteristics of the original Para-Sail, Configuration I, were determined, the next effort was devoted to the increase of the lift-drag ratio as well as to the establishment of the over-all performance characteristics. For these studies, Model I-48-47 was used.



RISER	LINE NO.	LINE LENGTH (INCLUDING RISER)
RIGHT FRONT	(1 → 5)	1.00 $D_d$
LEFT FRONT	(20 → 24)	1.00 $D_d$
RIGHT REAR	(6 → 12)	1.00 $D_d$
LEFT REAR	(13 → 19)	1.00 $D_d$
—	CENTERLINE	0.92 $D_d$

FIG. 35. SCHEMATIC PLANFORM OF CONFIGURATION I SHOWING SUSPENSION LINE ADJUSTMENTS FOR A 5x7 LINE CONFIGURATION.

### The Apex Region

As mentioned in Part A of Section IV, a region of turbulent flow was found in the apex area as well as on the upper downstream side of the canopy. It was concluded that a reduction or elimination of this turbulence would result in an increase of the lift-drag ratio. Therefore, an attempt was made to cover the concave portion of the canopy caused by the pull from the center line. The high porosity apex was covered with a circular piece of fabric supported by an internal suspension system which was attached to the center line. Figure 37 illustrates this model.

However, tests indicated that this measure did not significantly change the stable angle or the stability.

### Leading Edge Collapse

Also, from the tests conducted in Part A of this section, it was noticed that the leading edge collapses at angle of attack of approximately  $40^{\circ}$ . Therefore, portions of panels 1, 2, 22, 23 and 24 were removed in an effort to reduce the tendency of these panels to collapse. Figure 38 shows a schematic drawing of the modified canopy. Pendulum tests indicated that the collapse of the leading edge now occurred at higher angles of attack. However, the Para-Sail had lost over-all stability which was indicated through considerable oscillations about its stable angle of attack.

In an attempt to improve the stability of this version as well as to increase the stable angle, portions of the

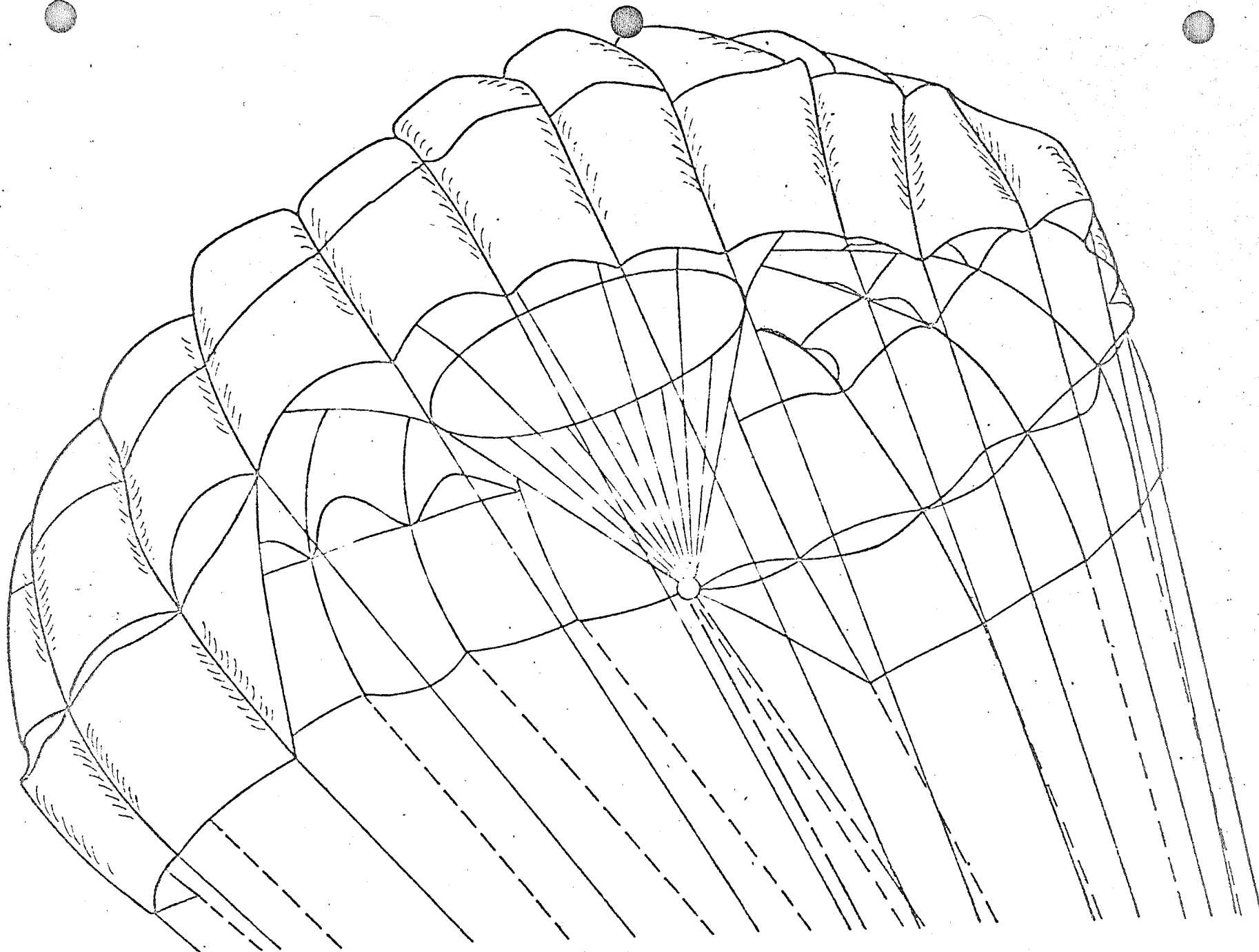


FIG 37. PARASAIL (I - 48 - 47) WITH MODIFIED APEX  
 $\alpha = 34^\circ$ ,  $L/D = .67$

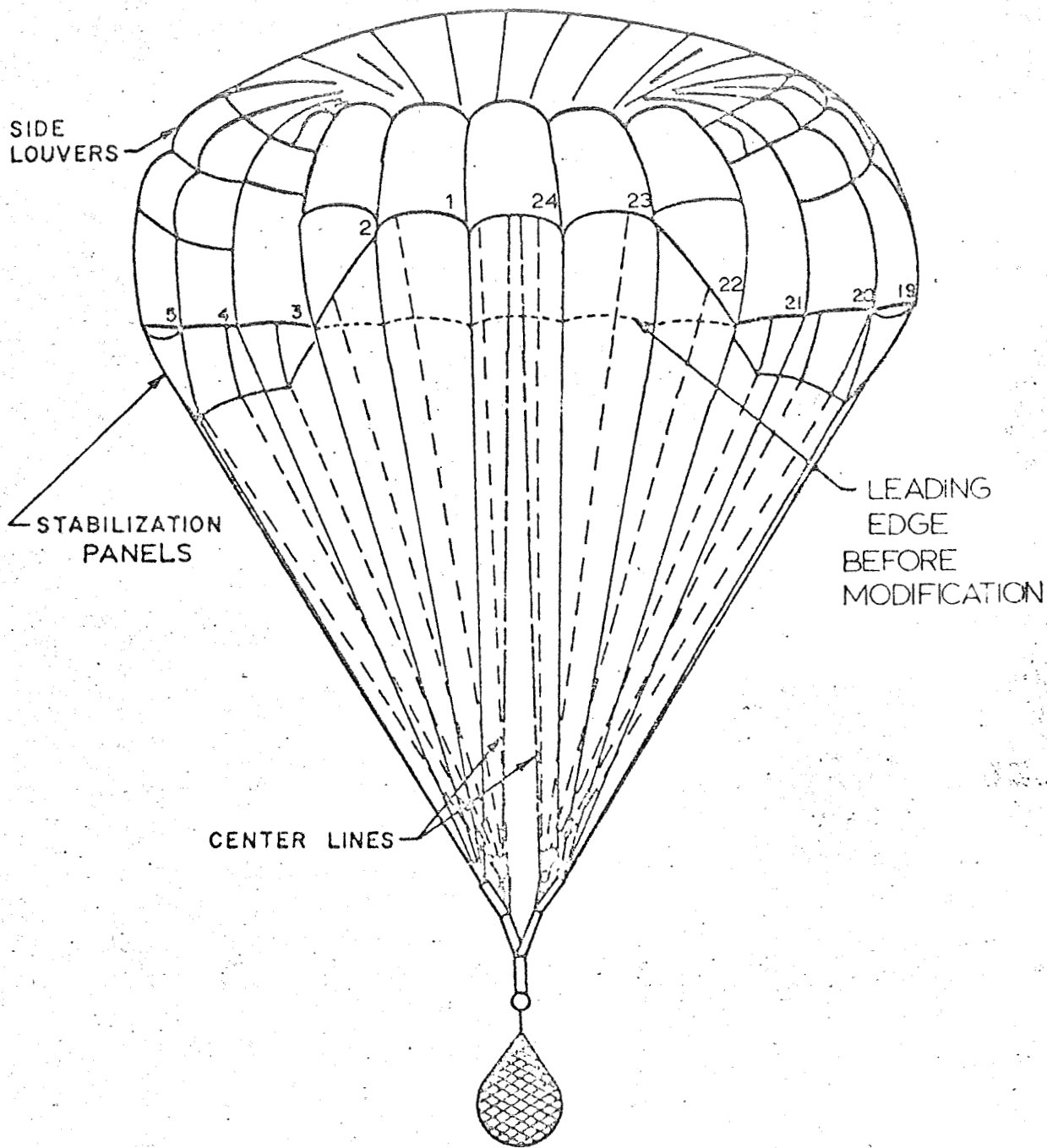


FIG 38. FRONT VIEW OF PARASAIL (I-48-47)  
WITH PORTIONS OF GORES 2, 1, 24, 23,  
AND 22 REMOVED

rear gores 10 through 14 were then removed. This modification is shown schematically in Fig 39. The reasoning behind this measure was to develop an exhaust jet which would push the canopy forward as well as to stabilize it.

Pendulum tests indicated a maximum stable angle of approximately  $40^{\circ}$  and satisfactory stability, which is an increase of  $5^{\circ}$  (see Fig 21).

Further pendulum tests on the same modified model, but without the stabilization panels, were made. This modification is illustrated in Fig 40. It was thought that removal of these panels would reduce the drag and therefore increase the lift-drag ratio. However, the experiments showed that the lift-drag ratio was not affected, however, the stability of the canopy was noticeably reduced.

#### Effect of Porosity and Removal of Cloth

All these efforts resulted merely in an increase of stable angle from  $34^{\circ}$  to  $40^{\circ}$ . The model used so far had a relatively high nominal porosity, namely,  $47 \text{ ft}^3/\text{ft}^2\text{-min}$ . The lower porosity model, I-32-4.67, already had a stable angle of attack of  $40^{\circ}$  before modification. Therefore, further tests were made with the lower porosity model, I-32-4.67.

The modifications were begun in a manner indicated by the preceding tests. First, portions of the front gores, numbers 1, 2, 22, 23 and 24, and portions of the rear gores, numbers 10 through 14, were removed.

This version showed in pendulum tests a stable

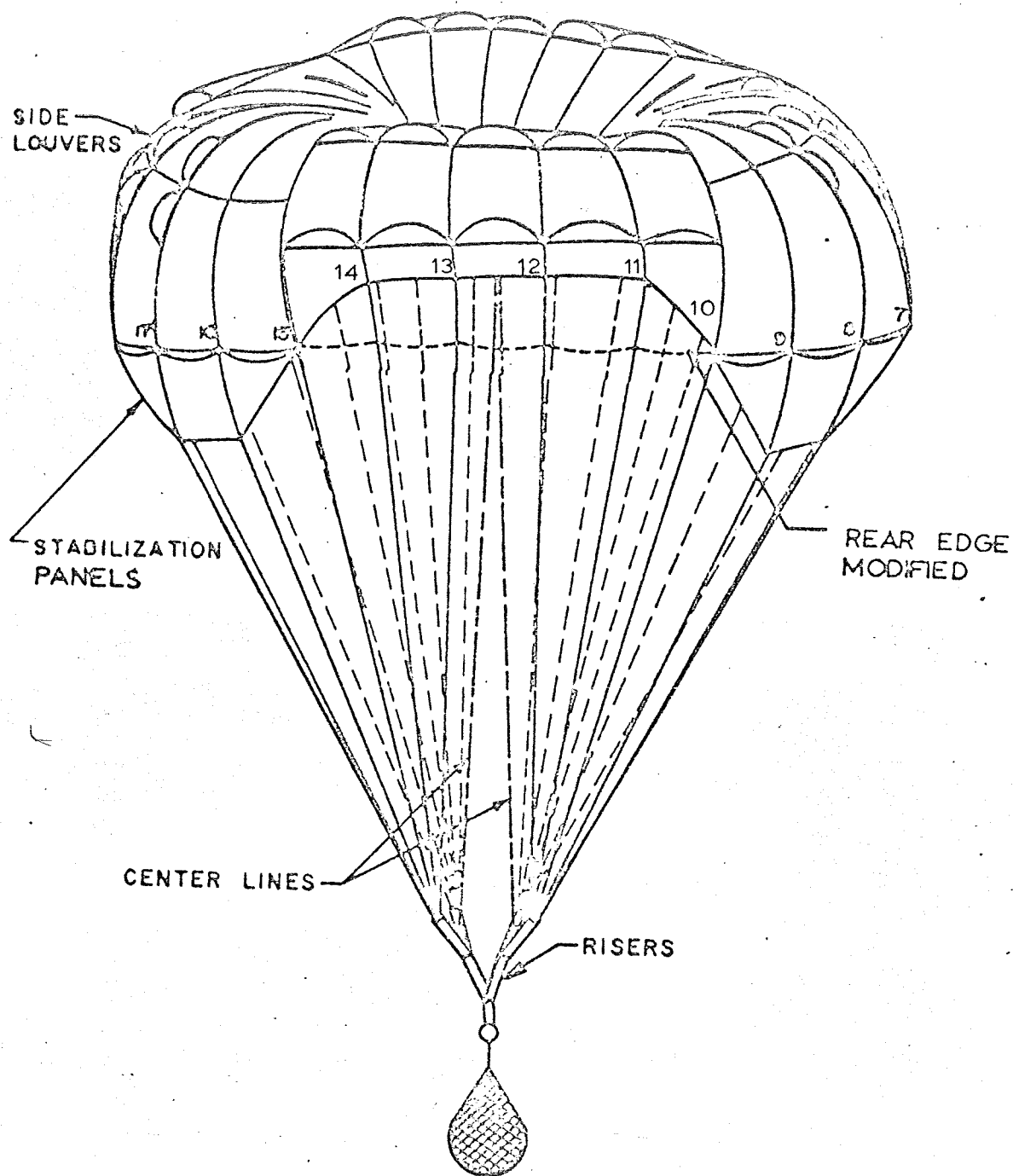


FIG 39. REAR VIEW OF PARASAIL (I-48-47)  
WITH PORTIONS OF GORES 10 - 14  
REMOVED ( $\alpha = 40^\circ$  L/D=.84)

angle of  $43^{\circ}$ , corresponding to a lift-drag ratio of 0.93. The same model in its original form had a stable angle of  $40^{\circ}$ . Visual observation indicated that the over-all stability of the modified model was very good.

#### Slots and Louvers on Low Porosity Model

Next, the slots and louvers of modified model I-32-4.67 were opened and closed. It was determined from this study that the front louvers had very little effect upon the general stability behavior of this model, but a slight tendency toward a higher L/D ratio was observed. Therefore, the front gores, numbers 1, 2, 22, 23 and 24, were replaced by solid gores similar to those of a solid flat canopy. Through this measure, the front gores became smooth surfaces.

Pendulum tests were then conducted and it was found that, although the stability was slightly decreased, the stable angle was increased to  $47^{\circ}$ , corresponding to a lift-drag ratio of 1.07. The final shape of the modified model I-32-4.67 is shown in Fig 41.

Line length variations indicated, as was previously found, that the stable angle can be both increased and decreased by changing the length of the front risers with respect to the rear risers. Also, when the slots between the side stabilization panels and the canopy were closed, the stable angle increased. However, this was accompanied by a lateral oscillation in the order of  $\pm 20^{\circ}$ , therefore, the slots were reopened.

No further modifications were made on the model shown in Fig 41, since it appeared that the optimum stable angle had been reached. The new configuration, derived through modifications of Configuration I, shall be called Configuration II. In pendulum tests, it had a stable angle of  $47^{\circ}$ , corresponding to a lift-drag ratio of 1.07. It appeared promising enough to justify further aerodynamic investigations.

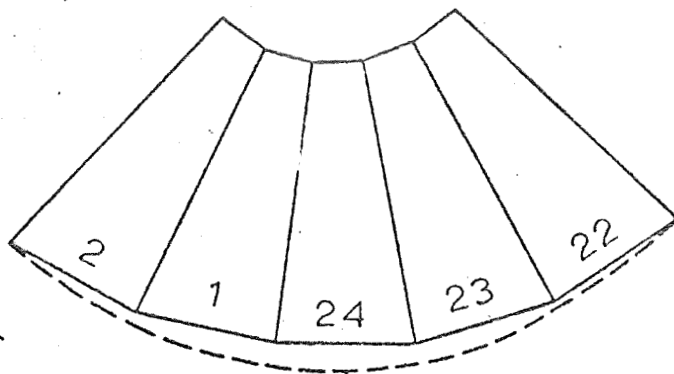
## V. INVESTIGATION OF CONFIGURATION II

The final modified version of Configuration I was called Configuration II. Figures 42 and 43 show, in dimensionless form, the differences in the patterns of the modified gores. A detailed description of the plan form of Configuration II is discussed in Section II and illustrated in Fig 5.

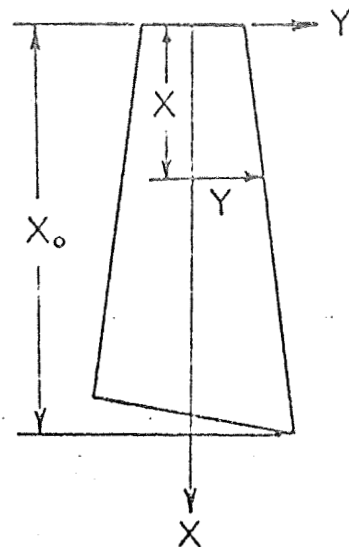
To determine the effect of porosity and the rate of descent on the stable angle, a series of tests were conducted on three models of Configuration II, differing merely in their nominal porosity.

The first series again made use of the pendulum method at velocities from 20 to 40 ft/sec. The results of these studies are shown in Fig 44. One notices that the stable angle increases both with decreasing porosity and slightly decreases with increasing velocity. The maximum stable angle which was reached amounts to  $47^\circ$ , representing an L/D ratio of 1.07.

To verify these results and to determine the stability of these three models at their respective stable angles, three-component tests were made. Figures 45 and 46 show Model II-24-4.67 in the wind tunnel and Figs 47 through 49 present their aerodynamic coefficients versus angle of attack. These results verify the trends observed in the pendulum tests. In particular, the stable angle of attack decreases for increasing porosity and the over-all stability decreases as the porosity increases. In general, the tangent forces of the lower porosity models is higher than the one of higher porosity models.



Skirt line for  
conventional solid  
flat parachute gore



Typical gore

GORE 24  $\frac{X_0}{D_d} = 0.325$

$\frac{X}{X_0}$	.1	.2	.3	.4	.5	.6	.7	.8	.9	1.0		
$\frac{Y}{X}$	.577	.356	.288	.252	.231	.216	.206	.198	.192	.188		

GORES 1 & 23  $\frac{X_0}{D_d} = 0.331$

$\frac{X}{X_0}$	.1	.2	.3	.4	.5	.6	.7	.8	.9	.98	.99	1.0
$\frac{Y}{X}$	.528	.335	.277	.241	.226	.208	.202	.195	.191	.188	.188	.187

GORES 2 & 22  $\frac{X_0}{D_d} = 0.335$

$\frac{X}{X_0}$	.1	.2	.3	.4	.5	.6	.7	.8	.9	.988	.993	1.0
$\frac{Y}{X}$	.514	.327	.268	.236	.222	.207	.200	.193	.187	.185	.184	.184

FIG 42. DIMENSIONLESS GORE PATTERN FOR  
FRONT OF CONFIGURATION II

FIG 43. DIMENSIONLESS GORE PATTERN FOR REAR SKIRT  
PANELS OF CONFIGURATION II

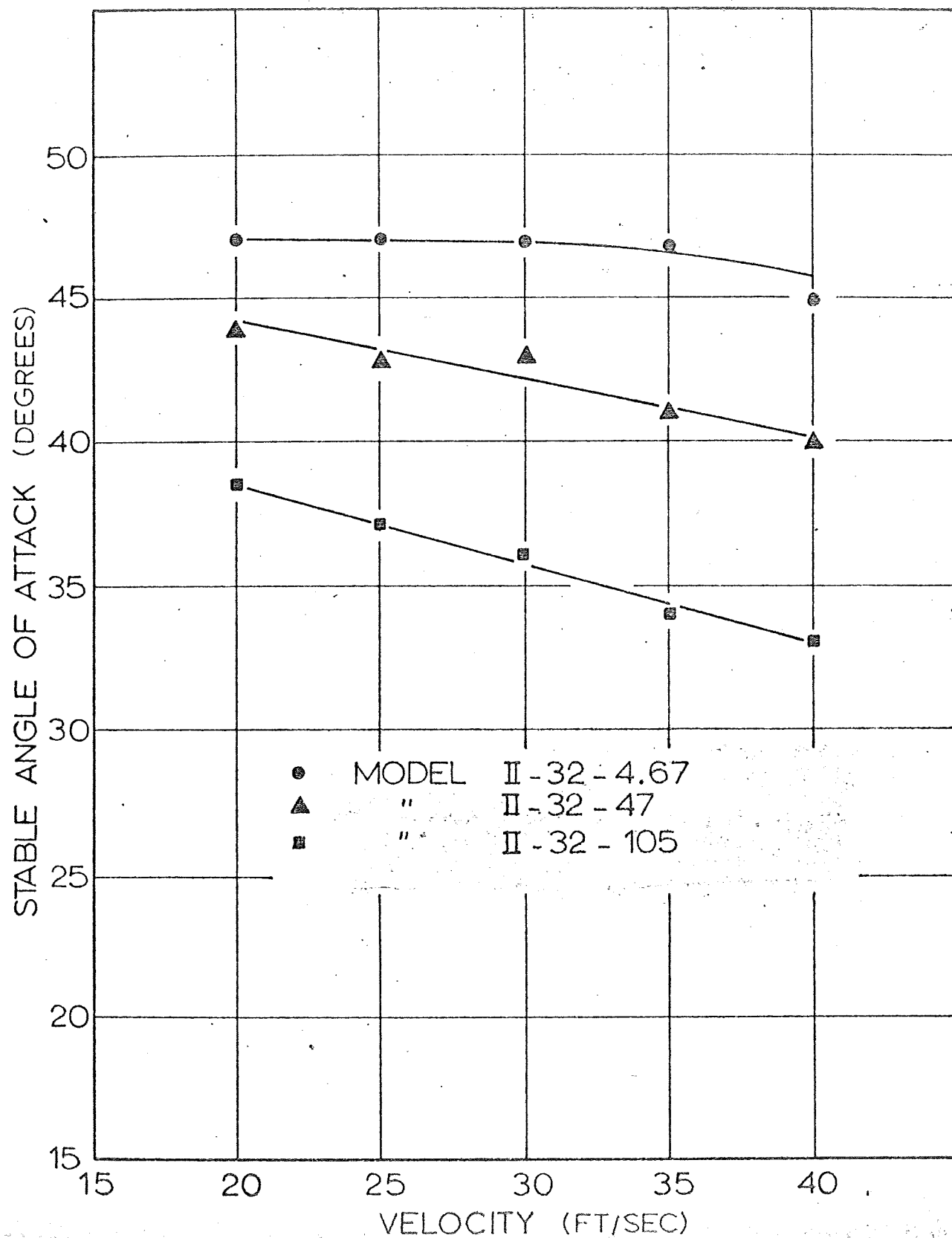


FIG 44, STABLE ANGLE OF ATTACK vs VELOCITY  
FOR CONFIGURATION II FOR VARIOUS  
NOMINAL POROSITIES

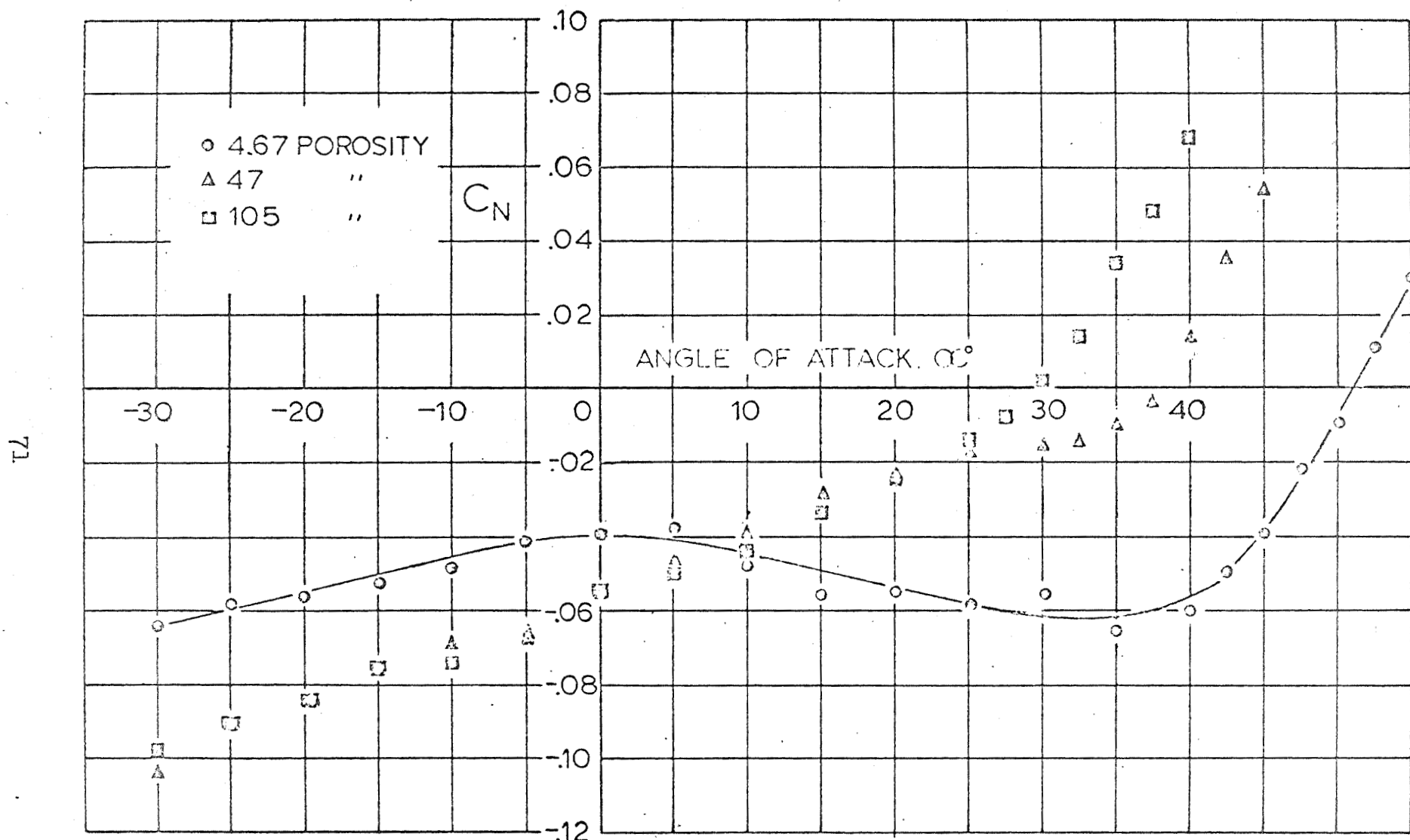


FIG 47. NORMAL FORCE COEFFICIENT vs ANGLE OF ATTACK  
FOR CONFIGURATION II (BASED ON TOTAL SURFACE  
AREA  $S_0$ ; REYNOLDS NUMBER  $= 8 \times 10^5$ ;  $D_0 = 24''$ )

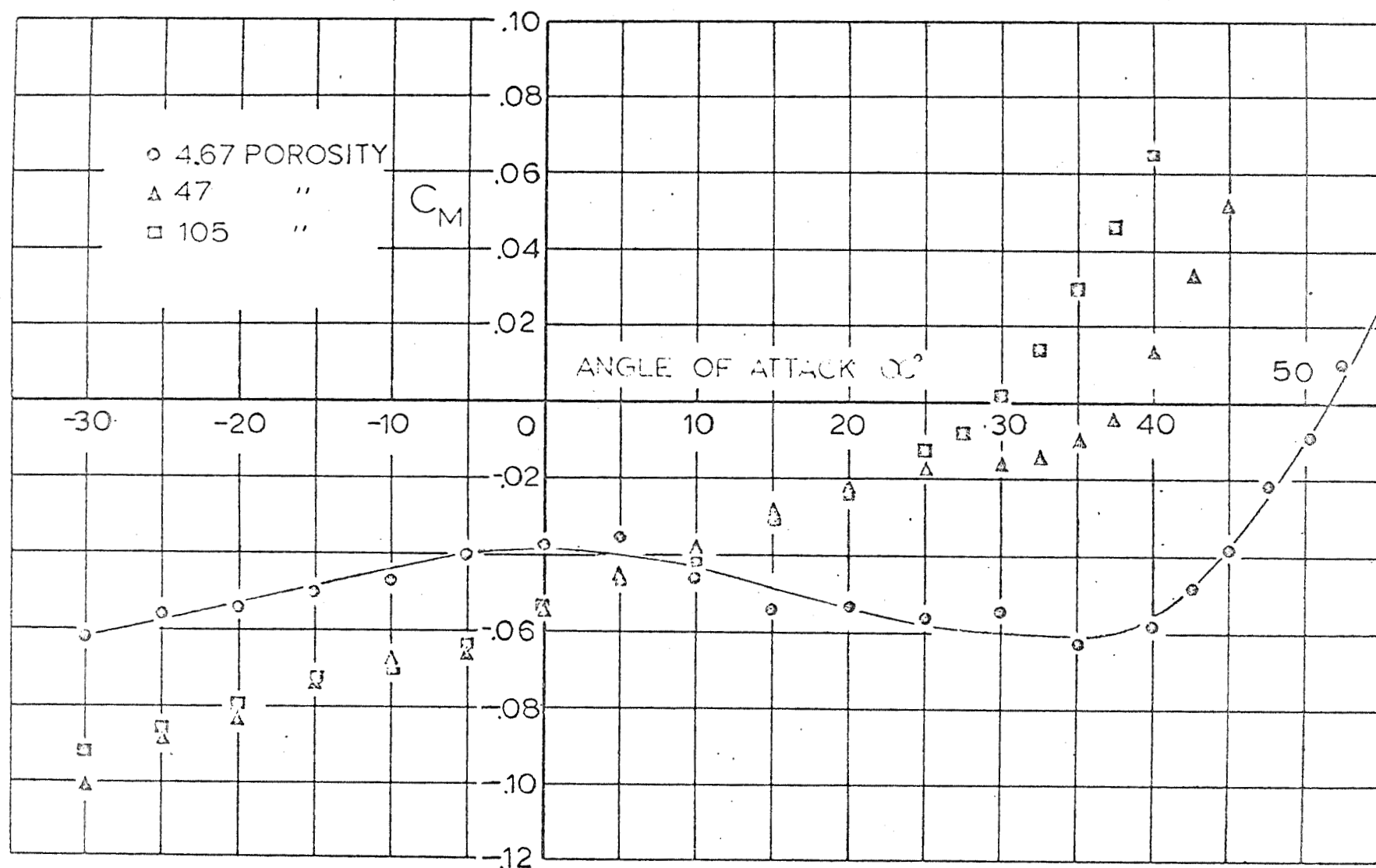


FIG 48. MOMENT COEFFICIENT vs ANGLE OF ATTACK FOR  
 CONFIGURATION II (BASED ON TOTAL SURFACE  
 AREA  $S_o$ ; REYNOLDS NUMBER  $= 8 \times 10^5$ ;  $D_o = 24''$ )

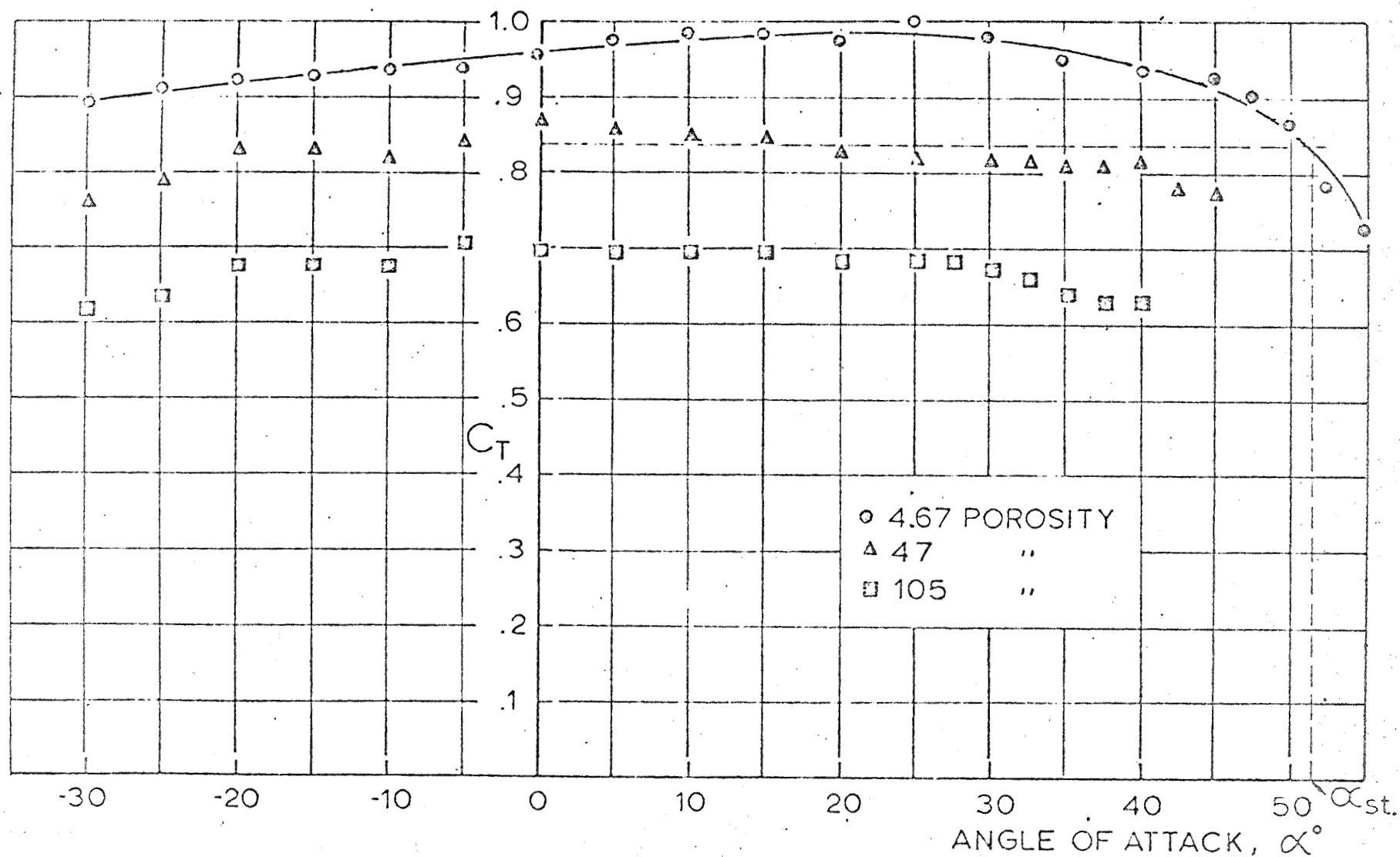


FIG 49. TANGENT FORCE COEFFICIENT vs ANGLE OF ATTACK  
FOR CONFIGURATION II (BASED ON TOTAL SURFACE  
AREA  $S_o$ ; REYNOLDS NUMBER =  $8 \times 10^5$ ;  $D_o = 24$  ")

Again, the stable angles determined from the three-component tests indicate larger angles. As before, the measurements in the pendulum tests may be considered as the lower limit of the stable angle of attack.

## VI. INVESTIGATION OF CONFIGURATIONS III AND IV

Configurations III and IV represent forms which evolved from a combination of experiences extracted from wind tunnel studies and from full size drop tests simultaneously conducted. Since the full size testing began with a version representing Configuration I, to which modifications were applied, Configurations III and IV are essentially modified versions of the Para-Sail Configuration I. Configuration II may be considered as merely an academic model, since full size drop tests with this configuration were never made.

### A. Configuration III

#### Opening Process

From drop tests of a full scale version of Configuration III, whose planform is shown in Fig 9, it was found that the parachute's opening process was erratic, in view of time and intermediate inflation forms. Thus, wind tunnel tests with Model III-48-4.67 were initiated to study and possibly to improve the opening characteristics of this configuration.

The opening process of this model was studied in a manner which schematically is shown in Fig 50. However, during the first series of tests no internal parachute was used. In these tests the Para-Sail model was suspended in the wind tunnel in reefed condition, while the flow was established. Then the reefing line was severed and the opening process recorded by means of a high speed motion picture camera. More details of this system have been described in Ref 3.

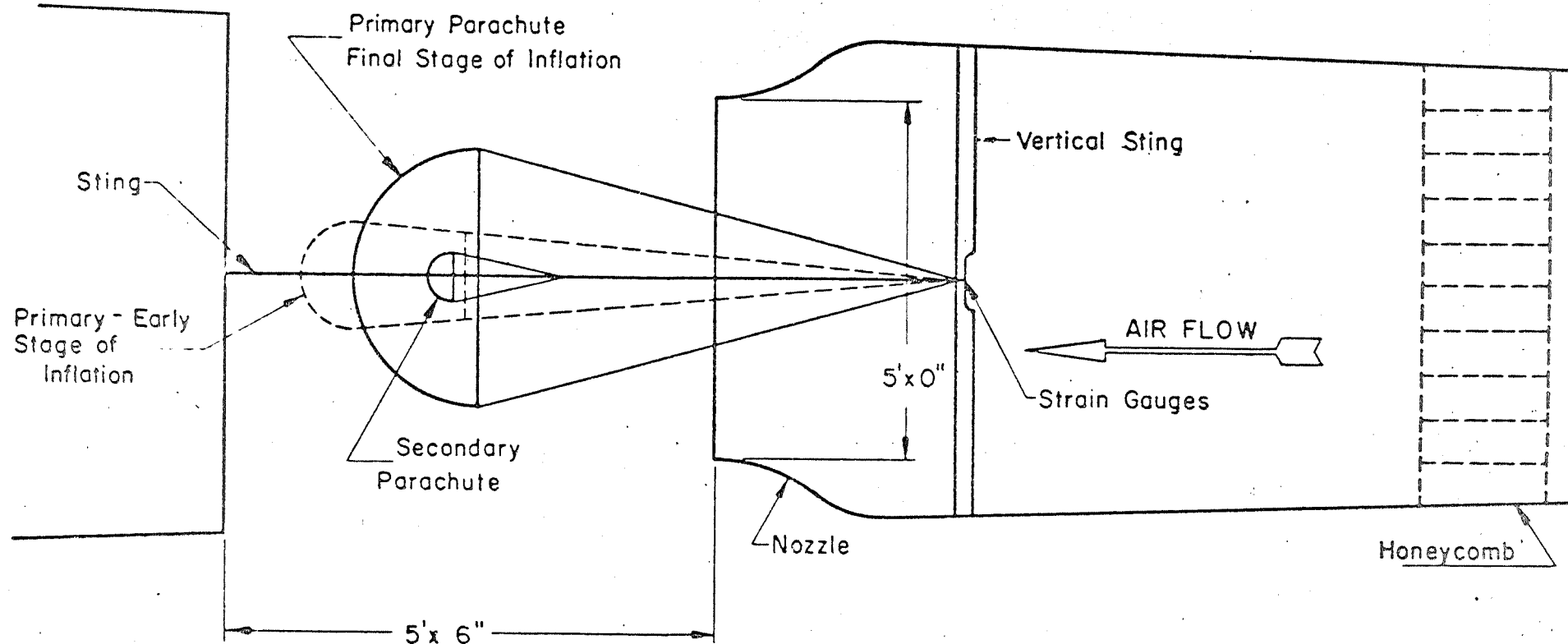


FIG. 50. TEST SECTION AND MODEL SUPPORT FOR OPENING SHOCK PROGRAM (INFINITE MASS CASE)

In this manner the following opening characteristics of Configuration III were observed:

- 1) During the opening process, the front panels bend inward, restricting the inlet opening and thereby prolonging the inflation time. The movement of the front panels was random, causing the entire filling process to be erratic.
- 2) The opening time was relatively long, and its standard deviation was relatively high.

These model experiments showed essentially the same features as had been observed in full size drop tests, and it was concluded that measures had to be introduced which would reduce the variation of the opening time and the random motion of the canopy cloth.

Reference 3 and related full size experiments have shown that a small parachute placed inside the larger primary parachute reduces the opening time and its standard deviation. Thus, a parachute having a projected diameter of 6.2" was employed as internal parachute with the 4 ft Para-Sail model. On the basis of Ref. 3 results, the internal parachute was placed at 3.8" behind the plane of the inflated skirt, corresponding to an  $L/D_0 = -8.33\%$ .

Inflation studies were then conducted and for comparison purposes models with and without internal parachutes were used. The experiments were made for the so-called infinite mass case wherein the relative velocity between the parachute and the free stream remains constant during the opening process.

Figures 50 and 51 show the arrangement of the parachute system in the wind tunnel.

In these tests, the average opening time of the Para-Sail without internal parachute was found to be approximately 0.21 seconds with a standard deviation of  $\pm 25\%$ . The average opening time with the internal parachute was 0.20 seconds with a variation from this average of  $\pm 5\%$ . Thus, the internal parachute reduced the opening time moderately but strongly standardized the opening process as indicated by the reduction of the standard deviation from  $\pm 25\%$  to  $\pm 5\%$ . However, merely a limited number of tests were made and more experiments are needed in order to optimize the size and location of the internal parachute. Furthermore, these tests were made with a Para-Sail having a center line. The conditions may change considerably when the internal parachute is used in connection with a Para-Sail without centerline.

#### Center of Pressure

The aerodynamic center line of Configuration III was determined in the manner described previously.

At the request of NASA, a 5 x 7 line configuration was used. The aerodynamic center line was found to be inclined toward the rear of the canopy at an angle of  $2^\circ$  with the parachute center line. Figure 52 shows these conditions graphically.

B. Configuration IV

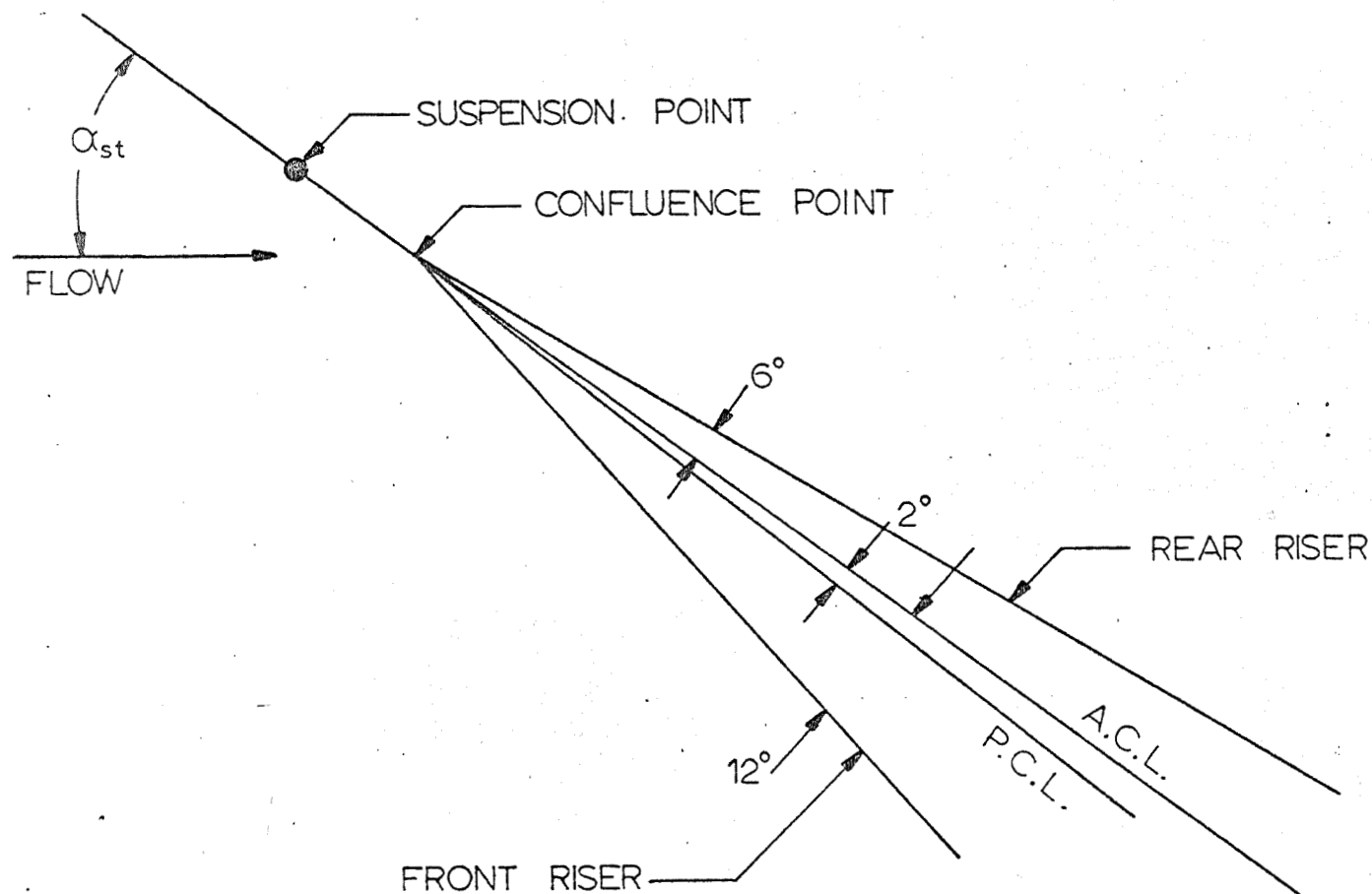


FIG 52. AERODYNAMIC CENTERLINE (A.C.L.) AND PARACHUTE CENTERLINE (P.C.L.) OF MODEL III-48-4.67 WITH AN UNATTACHED CENTERLINE (5 x 7 LINE CONFIGURATION  $V_{\infty} = 30$  ft/sec)

### Scoops and Length of Center Line

Drop tests were made with an 80 ft diameter version having a plan form representative of Configuration IV, Figure 11. However on the full size parachute only three (3) large scoops were arranged in the front gores, rather than nine (9) as shown in the figure. This was suggested by the prime contractor in an effort to improve the inflation characteristics. In addition to drop tests with this configuration with the purpose of studying the opening characteristics, wind tunnel tests were made to determine the effect these scoops made on the stable angle of attack. A four foot low porosity model, IV-48-4.67, was used.

Pendulum tests were conducted to determine the effect of the scoops combined with a center line variation upon the stable angle of attack. The results are shown in Table II. It can be seen that the scoops in all combinations decreased noticeably the glide angle. From this point of view, scoops cannot be recommended. It is also evident that the changes in the center line length affected the maximum stable angle very insignificantly.

### Centerline and Opening Characteristics

Full size drop tests showed that the scoops did not improve the opening characteristics. Since further undesirable opening features were recorded, the suitability of the center line was questioned. Therefore, new wind tunnel tests were made in order to determine at least qualitatively the effect of the center line on the parachute.

TABLE II. STABLE ANGLE OF ATTACK OF  
MODEL IV-48-4.67 WITH VARI-  
ATIONS IN THE CENTERLINE  
LENGTH AND NUMBER OF  
FRONT SCOOPS ( $V_{\infty}=25$  fps)

Centerline Extension Length (%)	NUMBER OF SCOOPS		
	9 large scoops $\alpha_{st} =$	18 smaller scoops $\alpha_{st} =$	no open scoops
0	32.9°	36.3°	41.0°
5.7	34.1°	35.9°	42.8°
10.3	34.0°	35.4°	43.3°
18.7	34.2°	35.7°	42.7°

The full size Para-Sail is always deployed in a reefed condition. During its inflation while reefed, it was observed that the leading side of the canopy is usually folded inward, which form remains also during the inflation after reefing line cutting. This method of inflation is undesirable in several aspects.

In order to reproduce this in the wind tunnel, a model, IV-48-4.67, with center line and reefed, was placed in the tunnel and held at various angles of attack.

Then in the next series of tests, the center line was removed and the experiments were repeated. The results, shown in Fig 53, emphasize the following points:

With the center line, the front of the parachute never inflated properly. Even at small angles of attack, the front side begins to collapse. Without center line, the front of the parachute inflates fully up to angles of attack as large as  $30^{\circ}$ . Even at angles of attack larger than  $45^{\circ}$  the front only partially collapsed. Details are shown in Fig 53.

From these tests, it is concluded that the center line influences the parachute's opening performance unfavorably.

#### Center of Pressure

The aerodynamic center line of Model IV-48-4.67 with a 9 x 9 suspension line configuration but without a center line was established. The method was the same as that employed

before. In accordance with Fig. 54, the aerodynamic center line is slightly inclined toward the rear of the canopy at an angle of approximately  $1^{\circ}$ . This indicates that in this version without a center line the total load is very uniformly divided between the front and rear risers.

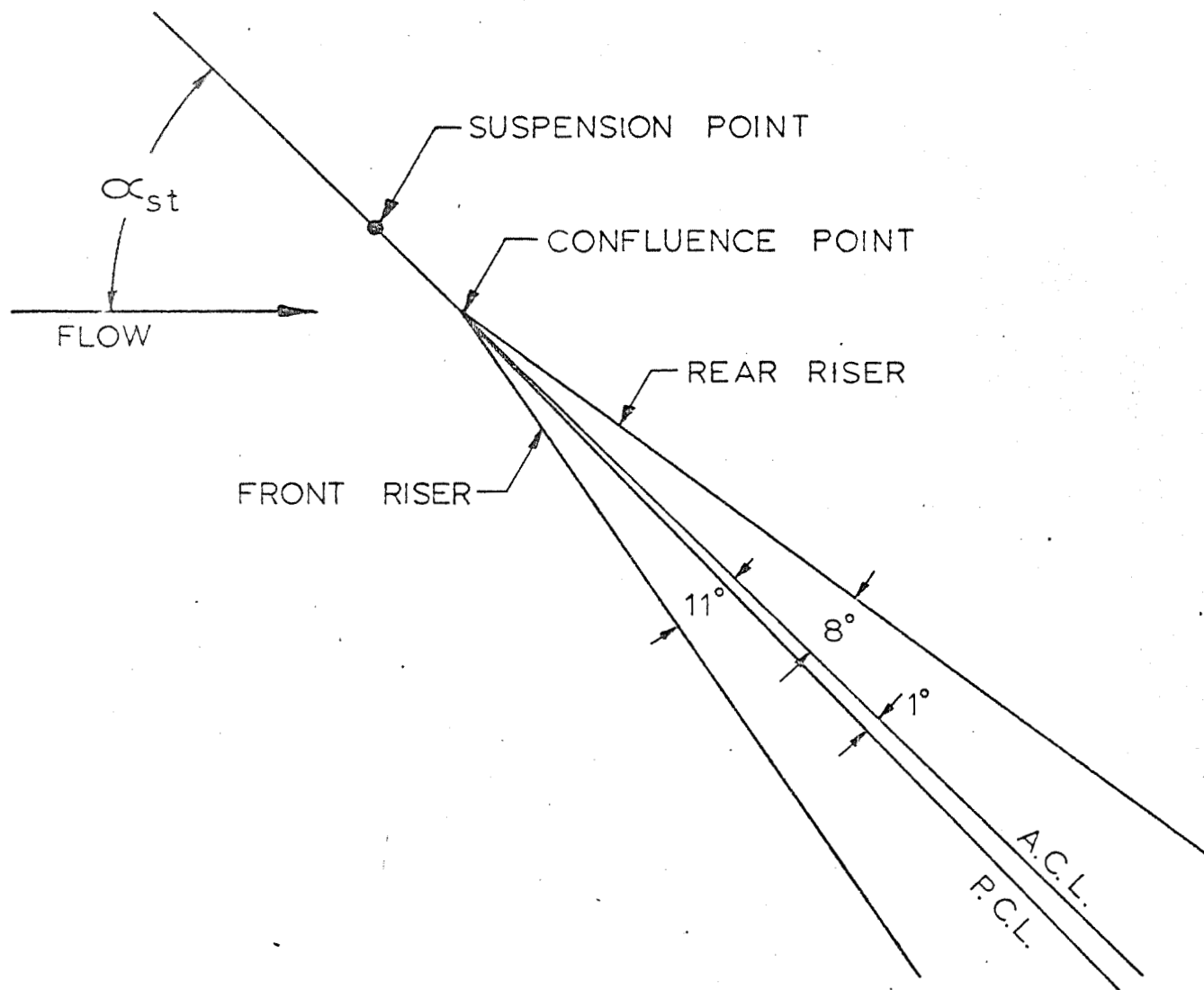


FIG 54. AERODYNAMIC CENTER LINE (A.C.L.) AND PARACHUTE CENTER LINE (P.C.L.) OF MODEL IV-48-4.67 WITH AN UNATTACHED CENTER LINE (9 x 9 LINE CONFIGURATION  $V_\infty = 30 \frac{\text{ft}}{\text{sec}}$ )

## VII. CONCLUSIONS

These reported studies indicate that Para-Sails can be built with a lift to drag ratio of higher than unity which are sufficiently stable about the three principal axes and that a certain lift to drag modulation is possible.

Figures 55 through 59 illustrate in condensed form the results of the studies involving the two more completely investigated Configurations I and II.

The investigation concerning Configurations III and IV were made in support of simultaneously conducted drop tests. They may be considered as guide lines for future developments.

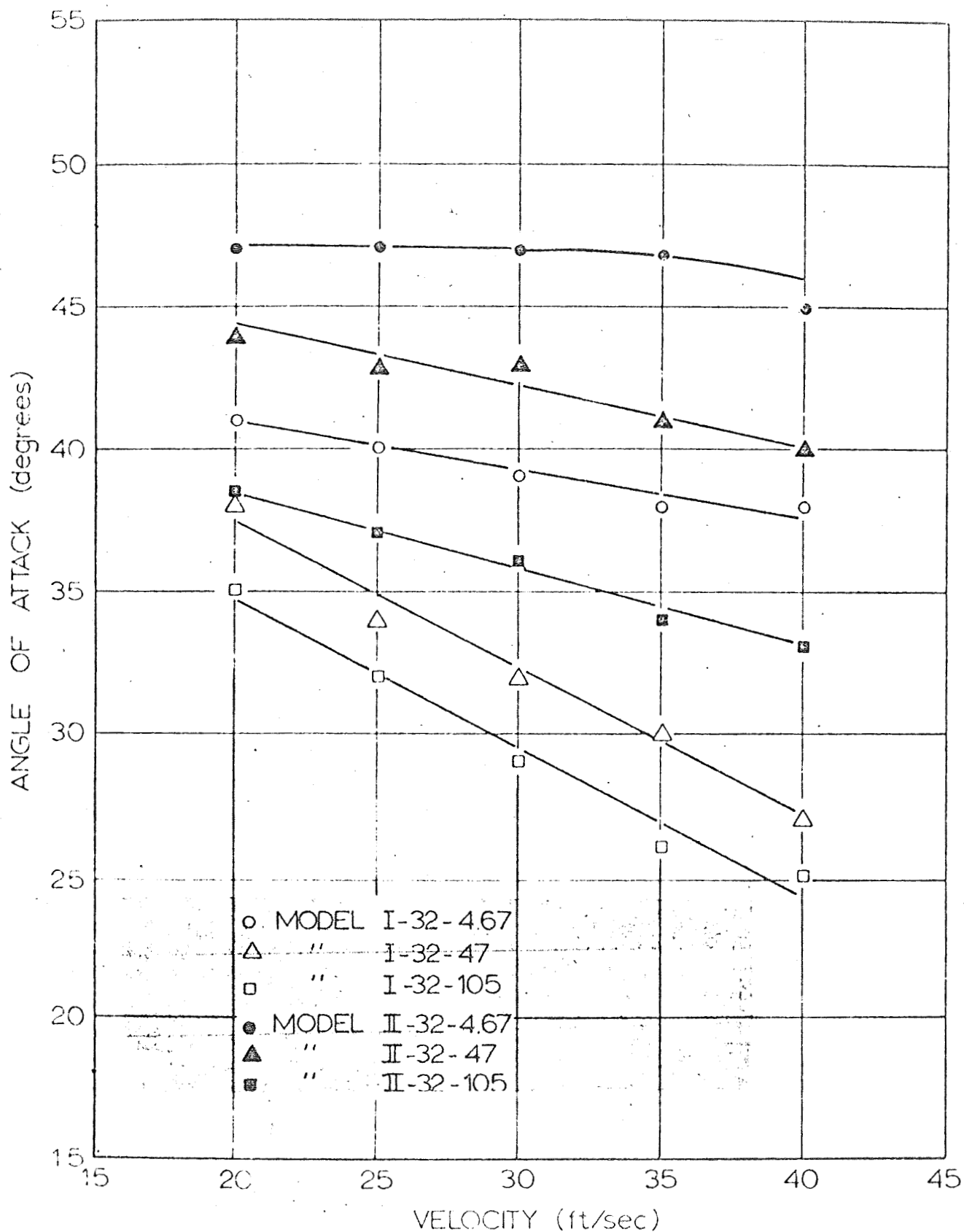


FIG 55. STABLE ANGLE OF ATTACK vs VELOCITY  
FOR CONFIGURATIONS I AND II FOR  
VARIOUS NOMINAL POROSITIES

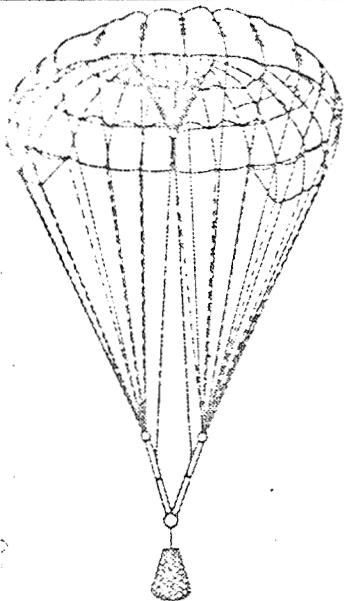
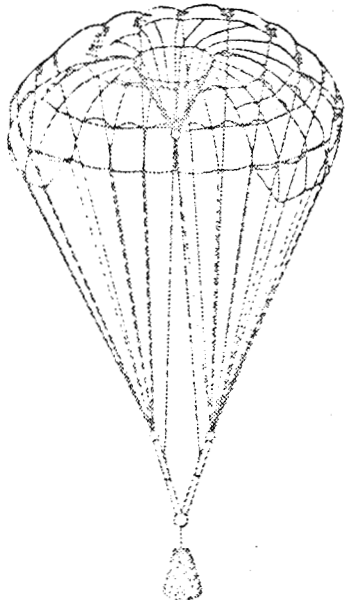
	MODIFICATIONS	RESULTS				
		$\alpha^\circ$	$\frac{L}{D}$	PITCH	ROLL	YAW
	HIGH POROSITY APEX REPLACED BY A FLAT COVER AND SUPPORTED WITH AN INTERNAL LINE STRUCTURE.	$34^\circ \pm 3^\circ$	0.68	$\pm 5^\circ$	$\pm 8^\circ$	$\pm 2^\circ$
	PORTIONS OF FRONT GORES (2,1,24,23,22) REMOVED AT THE SKIRT. THIS CONFIGURATION IS COMPLETELY UNSTABLE	—	—	—	—	—

FIG 56. RESULTS OF MODIFICATIONS OF PROTOTYPE PARASAIL I-48-47

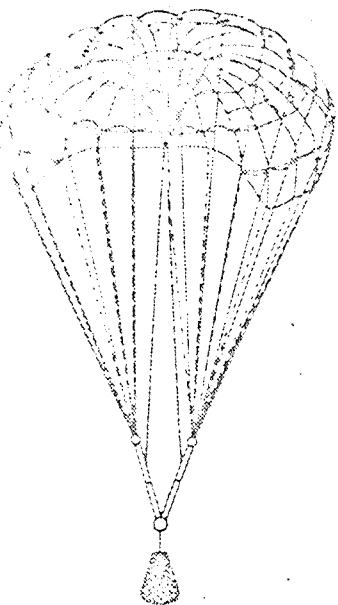
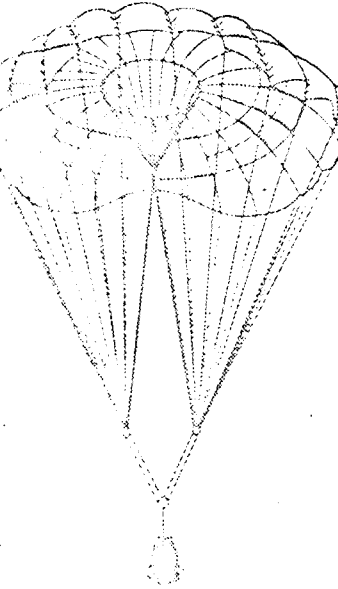
	MODIFICATIONS	RESULTS				
		$\alpha^\circ$	$\frac{L}{D}$	PITCH	ROLL	YAW
	PORTIONS OF REAR GORES (10-14) REMOVED AT THE SKIRT	$40^\circ$ $\pm 3^\circ$	0.84	$\pm 5^\circ$	$\pm 10^\circ$	$\pm 5^\circ$
	(FINAL CONFIGURATION) STABILIZATION PANELS REMOVED.	$40^\circ$ $\pm 3^\circ$	0.84	$\pm 5^\circ$	$\pm 15^\circ$	$\pm 10^\circ$

FIG. 57 RESULTS OF MODIFICATIONS OF PROTOTYPE PARASAIL I-48-47

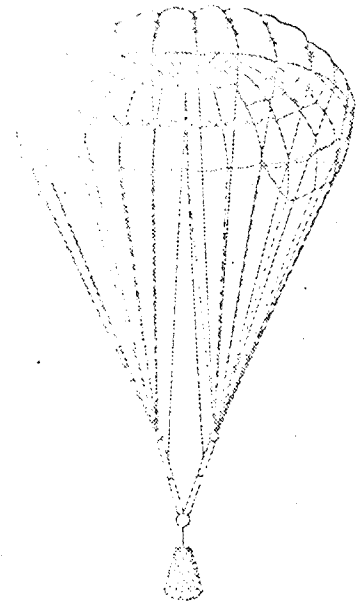
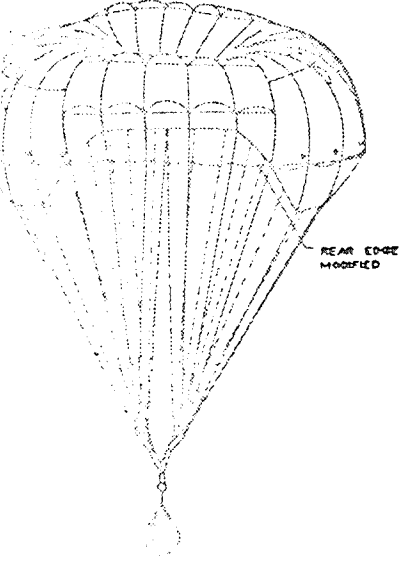
	MODIFICATIONS	RESULTS				
		$\alpha^\circ$	$\frac{L}{D}$	PITCH	ROLL	YAW
	PROTOTYPE PARASAIL (1-32) CENTER LINE LENGTHS=D.	$40^\circ$ $\pm 3^\circ$	0.84	$\pm 5^\circ$	$\pm 10^\circ$	$\pm 5^\circ$
	PORTIONS OF FRONT GORES (2,1,24,23,22) AND PORTIONS OF REAR GORES (10-14) REMOVED.	$43^\circ$ $\pm 3^\circ$	0.93	$\pm 5^\circ$	$\pm 12^\circ$	$\pm 5^\circ$

FIG. 58. RESULTS OF MODIFICATIONS OF PROTOTYPE PARASAIL I-32-467

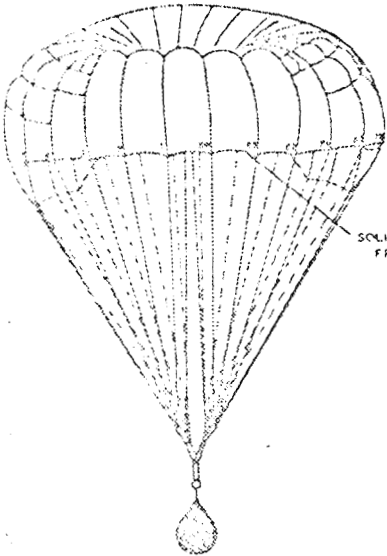
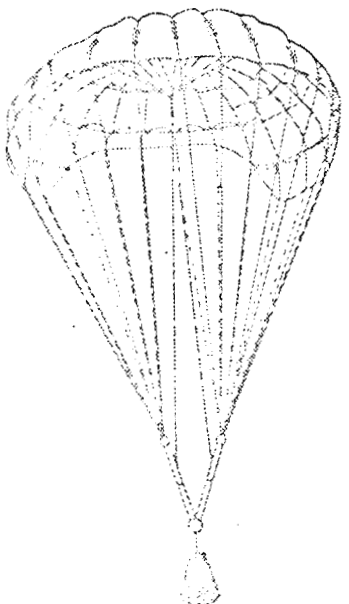
	MODIFICATIONS	RESULTS				
		$\alpha^\circ$	$\frac{L}{D}$	PITCH	ROLL	YAW
	FRONT FIVE GORES REPLACED WITH GORES FROM SOLID FLAT CANOPY	$47^\circ$ $\pm 3^\circ$	1.07	$\pm 5^\circ$	$\pm 15^\circ$	$\pm 5^\circ$
	FINAL CONFIGURATION (REMOVED PORTIONS OF REAR GORES AND REPLACED FRONT GORES WITH GORES FROM SOLID FLAT GORES)	$47^\circ$ $\pm 3^\circ$	1.07	$\pm 5^\circ$	$\pm 15^\circ$	$\pm 5^\circ$

FIG. 59. RESULTS OF MODIFICATIONS OF PROTOTYPE PARASAIL I-32-46

## REFERENCES

1. Heinrich, Helmut G. and Haak, Eugene L.: Stability and Drag of Parachutes With Varying Effective Porosity, ASD TR 62-100.
2. United States Air Force Parachute Handbook, ASD TR 61-579.
3. Heinrich, Helmut G. and Niccum, Ronald J.: A Method to Reduce Parachute Inflation Time With a Minor Increase of Opening Force, WADD TR 60-761.
4. Norman, Leland C.: NASA Program Apollo Working Paper No. 1118, Manned Spacecraft Center, Houston, Texas, May, 1964.

## APPENDIX

During the course of this study several sideline investigations were carried out, two of which appear to be worthwhile to record, namely, the relationship between line length and elliptical plan form and the effect of side stabilization panels.

### A. Line Lengths of the Eighty Foot Para-Sail and Their Relationship to an Elliptical Plan Form When Inflated

#### Notation

a	Semi-major diameter of canopy sketched from film
b	Semi-minor diameter of canopy sketched from film
A	Semi-major diameter of eighty foot Para-Sail
B	Semi-minor diameter of eighty foot Para-Sail
$l_s$	Length of suspension line and riser to confluence point of canopy (for sketch)
$L_s$	Length of suspension line and riser to confluence point of canopy (for eighty foot Para-Sail)
L	Perpendicular distance from the plane of the ellipse to the confluence point (for eighty foot Para-Sail)
$L_s'$	Longest suspension line needed to make the ellipse lie in one plane (for eighty foot Para-Sail)

$L_s$  Equals the difference between  $L_s$  and  $L_s'$   
(for eighty foot Para-Sail)

$l'$  Suspension line length necessary to make  
the elliptical circumference of the canopy  
mouth lie in a single plane.

Recorded Plan and Profile From

From the films of the eighty foot Para-Sail, sketches  
of both side and bottom views of the fully inflated canopy  
were obtained, as illustrated in Figs. 60 and 61.

The film showed that the skirt of the parachute had  
projected an elliptical shape, with a ratio of the semi-  
major ("a") to the semi-minor ("b") axes of 1.441. Therefore,  
the general equation for this ellipse is:

$$\frac{x^2}{(1.441 b)^2} + \frac{y^2}{b^2} = 1$$

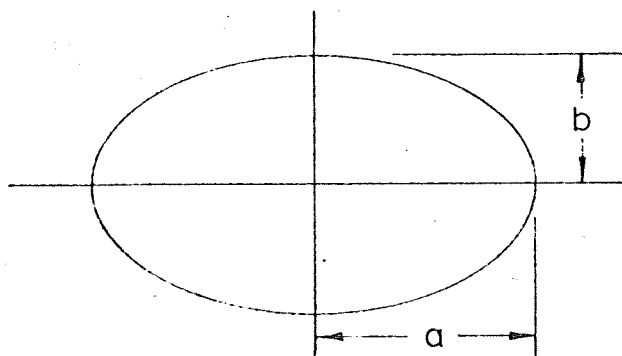


FIG. 60. PLAN FORM OF THE INFLATED 80 FT PARA-SAIL

The front and side view sketches of the Para-Sail indicate a certain distortion of the canopy which is caused by the fact that all suspension lines are of equal length. Assuming a fixed minor axis and given suspension lines in the middle of the front and the rear, one can compute the length of all suspension lines in such a manner that the projected plan form of the Para-Sail would form an ellipse in a plane.

The semi-minor and semi-major axes were found to be 23 and 33.2 feet, respectively. From this and the condition above, one can determine the longest required suspension lines if the shortest ones in mid front and mid rear are  $L_s = 68.1$  feet. It can be shown that the longest lines would be placed on the outside tips and should have a length of  $L_s = 72.2$  feet.

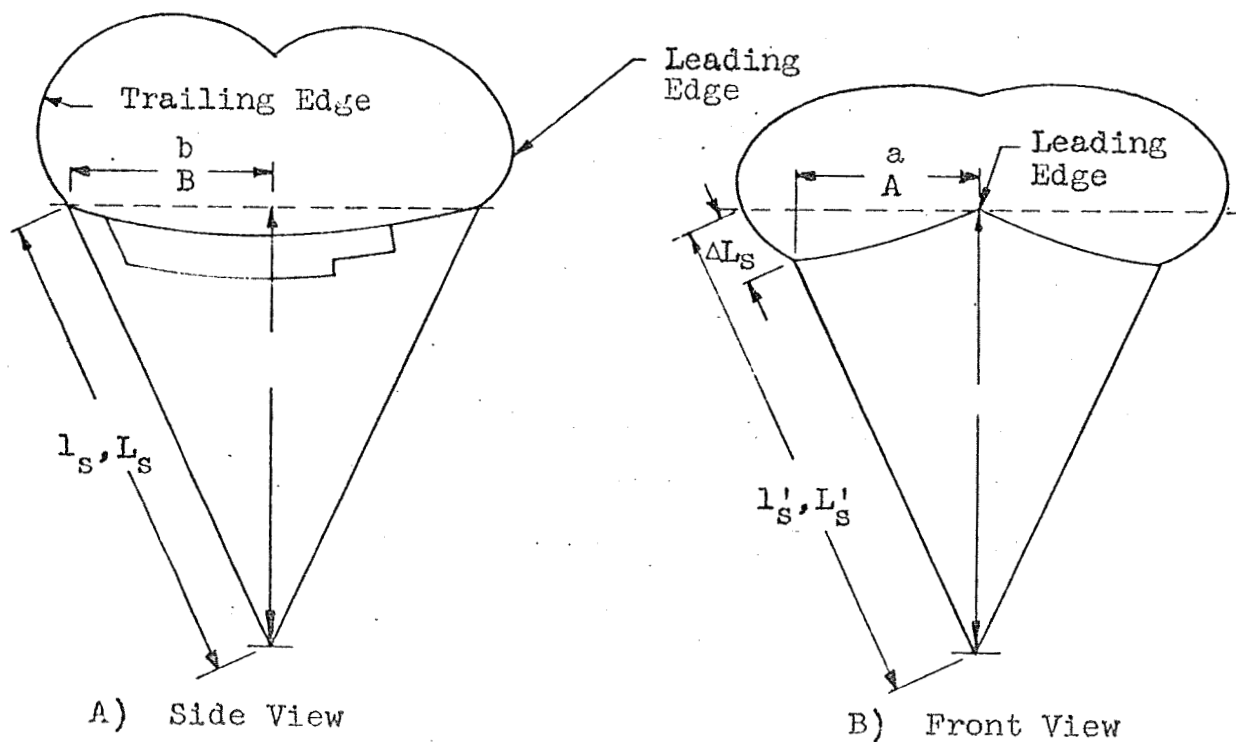


FIG. 61. PROFILES OF THE INFLATED 80 FT PARA-SAIL

By means of the general equation of the ellipse, one could determine the proper length of all lines, which would vary between 68.1 and 72.2 feet.

From the theory of the lifting surface, it can be seen that also for a parachute an elliptical plan form is very advantageous for the development of a high lift to drag ratio.

#### B. Investigation of Stabilization Panels

Tests were conducted on Model IV-48-4.67 to study the effect stabilization panels have on drag and stability. For these tests, the parachute was suspended from the pendulum device described before.

The parachute was first studied without any alterations. Then, the stabilization panels were trimmed to conform with the current configuration of the 80 foot Para-Sail. Finally, they were removed completely.

The tests indicated the following results:

- 1) the lift to drag ratio was not appreciably affected as the panels were removed;
- 2) the drag of the canopy appeared to remain constant;
- 3) no significant change in the stability was observed even with complete removal of stabilization panels.

The side panels may, however, have an effect through their interaction with the elliptical plan form as well as with the canopy loading. These aspects have not been investigated.